

Dear Editor,

Thank you very much for taking the time to handle the review process of our manuscript and providing useful recommendations!

With respect,

M. Kulikov, A. Nechaev, M. Belikovich, T. Ermakova, and A. Feigin

Response to the comments on the paper by Referee #1

Dear Referee,

We appreciate you taking the time to review our manuscript and we are grateful for your comments and constructive recommendations!

With respect,

M. Kulikov, A. Nechaev, M. Belikovich, T. Ermakova, and A. Feigin

**List of technical corrections:**

Below Referee's comments are in *blue italic*, our comments are in black.

1. *Line 38 "validate results of remote or in situ measurements". One should carefully consider the wording here. Models do not validate measurements. Perhaps "compare with results of measurements" is what is meant.*

Corrected. "validate" was replaced with "evaluate". See line 38 below.

2. *Line 193 "COMMA-IAP middle atmosphere dynamics" needs some explanation. This is also confusing because the previous paragraph states that the model dynamics is from CMAM.*

To avoid the confusion we deleted the sentence about COMMA-IAP model. See lines 194-196. The citations from the sentence were moved to the first sentence in Section 2. See lines 163-165.

3. *Line 241 "dashed area" looks like a shaded area or gray area in the figure.*

Corrected. "dashed area" was replaced by "gray area". As it is indeed looks like gray area in print. See line 242.

4. The acknowledgments were changed. See lines 432-434. The references were corrected. See lines 448, 462, 464, 499, 622, 736-738, 754-756, 778-783.

1 **Technical Note: Evaluation of simultaneous measurements of mesospheric OH, HO<sub>2</sub>, and O<sub>3</sub>**  
2 **under photochemical equilibrium assumption: Statistical approach**

4 Mikhail Yu. Kulikov<sup>1</sup>, Anton A. Nечаев<sup>1</sup>, Mikhail V. Belikovich<sup>1</sup>, Tatiana S. Ermakova<sup>1</sup>, and  
5 Alexander M. Feigin<sup>1</sup>

7 <sup>1</sup>Institute of Applied Physics of the Russian Academy of Sciences, 46 Ulyanov Str., 603950 Nizhny  
8 Novgorod, Russia

10 Correspondence to: Mikhail Yu. Kulikov (mikhail\_kulikov@mail.ru)

12 **Abstract**

14 The Technical Note presents a statistical approach to evaluating simultaneous measurements of  
15 several atmospheric components under the assumption of photochemical equilibrium. We consider  
16 simultaneous measurements of OH, HO<sub>2</sub>, and O<sub>3</sub> at the altitudes of the mesosphere as a specific  
17 example and their daytime photochemical equilibrium as an evaluating relationship. A simplified  
18 algebraic equation relating local concentrations of these components in the 50-100 km altitude  
19 range has been derived. The parameters of the equation are temperature, neutral density, local  
20 zenith angle, and the rates of 8 reactions. We have performed a one-year simulation of the  
21 mesosphere and lower thermosphere using a 3D chemical-transport model. The simulation shows  
22 that the discrepancy between the calculated evolution of the components and the equilibrium value  
23 given by the equation does not exceed 3-4% in the full range of altitudes independent of season or  
24 latitude. We have developed the technique of statistic Bayesian evaluation of simultaneous  
25 measurements of OH, HO<sub>2</sub> and O<sub>3</sub> based on the equilibrium equation taking into account the  
26 measurement error. The first results of application of the technique to MLS/Aura data are  
27 presented in this Technical Note. It has been found that the satellite data of HO<sub>2</sub> distribution  
28 regularly demonstrates essentially lower altitudes of mesospheric maximum of this component.  
29 This has also been confirmed by model HO<sub>2</sub> distributions and comparison with offline retrieval of  
30 HO<sub>2</sub> from the daily zonal means MLS radiance.

32     1. Introduction

33

34     A prominent feature of the atmospheric photochemical systems is the presence of a large number  
35     of chemical components with short lifetime and concentrations close to stable photochemical  
36     equilibrium at every instant. The condition of balance between their sources and sinks is described  
37     by a system of algebraic equations. This system can be used to determine characteristics of hard  
38     to measure atmospheric species through other measurable components, ~~validate evaluate~~ results  
39     of remote or *in situ* measurements, estimate reaction rates usually known with significant  
40     uncertainty, and to understand processes and chemical reactions that influence variability of the  
41     most important atmospheric components, e.g. ozone, in the geographical region of interest.

42         This approach has found wide application:

43         (1) in 3D chemical transport models that include a large set of physical and chemical  
44     processes with a broad spectrum of spatio-temporal scales. In particular, the chemical family  
45     concept is widely used for simulating gas phase photochemistry of the lower and middle  
46     atmosphere (e.g., Douglass et al., 1989; Kaye and Rood, 1989; Rasch et al., 1995), when transport  
47     is taken into account only for the concentration of a chemical family, while relative concentrations  
48     of the constituent fast components are calculated from the instantaneous stable equilibrium  
49     condition. Complemented with the Henry law (e.g., Djouad et al., 2003; Tulet et al., 2006) in  
50     multiphase models, this approach markedly saves calculation time and increases the overall  
51     stability of the numerical scheme. Moreover, the use of the photochemical equilibrium condition to  
52     simulate fast components dynamics reduces the phase space dimension of box models  
53     significantly (e.g., Kulikov and Feigin, 2014), allowing a comprehensive analysis of nontrivial  
54     nonlinear dynamic properties of various atmospheric photochemical systems (e.g., Feigin and  
55     Konovalov, 1996; Feigin et al., 1998; Konovalov et al., 1999; Konovalov and Feigin, 2000; Kulikov  
56     et al., 2012).

57         (2) in investigations of the chemistry of the surface layer and free troposphere in different  
58     regions (over megalopolises, in rural areas, in the mountains, over the seas) based on  
59     measurements of nitrogen species, peroxy radicals, ozone, aerosols, and other components aimed  
60     at understanding processes impacting the surface ozone formation and air quality. The equilibrium  
61     condition is most frequently used for nitrogen species. For example, Chameides (1975) proposed a  
62     model for determining the vertical distribution of odd nitrogen, in which the  $\text{HNO}_3$  profile could be

63 deployed to retrieve profiles of five other components (NO, NO<sub>2</sub>, NO<sub>3</sub>, N<sub>2</sub>O<sub>5</sub>, and HNO<sub>2</sub>) from their  
64 photochemical equilibrium condition. In the paper by Stedman et al. (1975) the equation for NO<sub>2</sub>  
65 equilibrium that accounted only for the main source and sink of this component was applied to  
66 determine the photodissociation constant J(NO<sub>2</sub>). A more accurate equation for the NO<sub>2</sub> equilibrium  
67 was used by Crawford et al. (1996) and Kondo et al. (1996) to determine the NO<sub>2</sub>/NO partitioning  
68 and NO<sub>x</sub>, allowing, in particular, investigating the spatial distribution of NO<sub>x</sub>/NO<sub>y</sub> over the Pacific.

69 Night-time equilibrium in the NO<sub>2</sub>-NO<sub>3</sub>-N<sub>2</sub>O<sub>5</sub> system is used to determine surface layer N<sub>2</sub>O<sub>5</sub>  
70 concentration, equilibrium constant of this system, equilibrium partitioning between NO<sub>3</sub> and N<sub>2</sub>O<sub>5</sub>,  
71 and loss coefficients of NO<sub>3</sub>, N<sub>2</sub>O<sub>5</sub> and NO<sub>x</sub> (Martinez et al., 2000; Brown et al., 2003; Crowley et  
72 al., 2010; McLaren et al., 2010; Benton et al., 2010; Sobanski et al., 2016).

73 Platt et al. (1979) used the CH<sub>2</sub>O photochemical equilibrium condition to analyse results of  
74 simultaneous measurement of CH<sub>2</sub>O, O<sub>3</sub> and NO<sub>2</sub> and to identify mechanisms of CH<sub>2</sub>O formation  
75 over rural areas and in maritime air. In the papers by Ko et al. (2003), Cantrell et al. (2003),  
76 Penkett et al. (1997), Penkett et al. (1998) algebraic expressions derived from equilibrium  
77 conditions for H<sub>2</sub>O<sub>2</sub>, peroxy radicals and nitrogen species were used to determine equilibrium  
78 values of peroxide concentration, total peroxy radical level, and NO/NO<sub>2</sub> ratio, and to diagnose the  
79 ozone production and loss levels in clean or polluted troposphere.

80 (3) in stratospheric chemistry studies, including determination of a critical parameter in  
81 catalytic cycles of ozone destruction in the polar stratosphere. In particular, the equilibrium  
82 condition for ClO and Cl<sub>2</sub>O<sub>2</sub> along with the measurement data of daytime and night-time  
83 concentrations of these components in the polar stratosphere are used to evaluate the temperature  
84 dependence of the ClO concentration, reaction constants determining the  
85 ClO + ClO + M  $\leftrightarrow$  Cl<sub>2</sub>O<sub>2</sub> + M equilibrium, and the photolysis rate of Cl<sub>2</sub>O<sub>2</sub> (Ghosh et al., 1997;  
86 Avallone et al., 2001, Solomon et al., 2002; Stimpfle et al., 2004; von Hobe et al., 2005; Berthet et  
87 al., 2005; Butz et al., 2007; von Hobe et al., 2007; Kremser et al., 2011; Sumińska-Ebersoldt et al.,  
88 2012; Wetzel et al., 2012).

89 Pyle et al. (1983) proposed a method for derivation of the OH concentration from satellite  
90 infrared measurements of NO<sub>2</sub> and HNO<sub>3</sub> using a simple algebraic relation following from the  
91 equilibrium condition for HNO<sub>3</sub>. Algorithms for retrieving distributions of OH and HO<sub>2</sub> from the  
92 satellite measurement data of O<sub>3</sub>, NO<sub>2</sub>, H<sub>2</sub>O, HNO<sub>3</sub> by LIMS/Nimbus 7 and UARS with the help of  
93 algebraic models following from the photochemical equilibrium of O<sub>x</sub>, HO<sub>x</sub> and HNO<sub>3</sub> components

were proposed by Pyle and Zavody (1985), Pickett and Peterson (1996). It is also worthy of note that similar models are widely used for calculating concentrations of components with a short lifetime (e.g. O(<sup>1</sup>D) and OH) and subsequent evaluating vertical distributions of eddy diffusivity from measurements of trace gas concentration profiles (see, e.g., Massie and Hunten, 1981).

Kondo et al. (1988) made use of the photochemical equilibrium between NO and NO<sub>2</sub> for understanding diurnal variations of NO concentration measured during aircraft flights. In the paper by Webster et al. (1990) simultaneous *in situ* balloon-borne measurements of NO, NO<sub>2</sub>, HNO<sub>3</sub>, O<sub>3</sub> and N<sub>2</sub>O and the photochemical equilibrium condition for various nitrogen components were used to determine OH, N<sub>2</sub>O<sub>5</sub> and NO<sub>y</sub> concentrations. A similar approach was employed by Kawa et al. (1990), who obtained NO<sub>2</sub>, N<sub>2</sub>O<sub>5</sub>, ClNO<sub>3</sub>, HNO<sub>3</sub> and OH concentrations from aircraft measurements of NO, ClO and O<sub>3</sub> concentrations. Hauchecorne et al. (2010) found that NO<sub>3</sub> concentration measured by GOMOS/ENVISAT positively correlates with temperature at altitudes up to 45 km in the region where NO<sub>3</sub> is in chemical equilibrium with O<sub>3</sub>. Funke et al. (2005) used NO and NO<sub>2</sub> stable-state photochemistry to verify correctness of the new approach of retrieving distributions of those component from MIPAS/ENVISAT measurement data. Marchand et al. (2007) proposed a method to retrieve the temperature distribution in the stratosphere between 30 km and 40 km from O<sub>3</sub> and NO<sub>3</sub> measurements by GOMOS with the help of a simple equation derived from the night-time NO<sub>3</sub> chemical equilibrium.

(4) in investigations of the chemistry of O<sub>x</sub>–HO<sub>x</sub> components and atmospheric glows in the mesosphere and MLT area. In particular, Kulikov et al. (2006, 2009) proposed algorithms for the simultaneous retrieval of O, H, HO<sub>2</sub> and H<sub>2</sub>O from joint OH and O<sub>3</sub> satellite measurement, in which the assumption of photochemical equilibrium of O<sub>3</sub>, OH, and HO<sub>2</sub> was utilized. For several decades the assumption of the photochemical equilibrium of ozone (PEO) was widely used to determine distributions of atomic oxygen and atomic hydrogen at altitudes of the MLT via satellite and rocket measurement of ozone concentration and airglow emissions (e.g., Evans and Llewellyn, 1973; Good, 1976; Pendleton et al., 1983; McDade et al., 1985; McDade and Llewellyn, 1988; Evans et al., 1988; Thomas, 1990; Llewellyn et al., 1993; Llewellyn and McDade, 1996; Mlynczak et al., 2007, 2013a, 2013b, 2014; Smith et al., 2010; Siskind et al., 2008, 2015). Russell and Lowe (2003) applied PEO to infer the seasonal and global climatology of atomic oxygen using WINDII/UARS. PEO was deployed to investigate hydroxyl emission mechanisms, morphology, and variability in the upper mesosphere – lower thermosphere region (Marsh et al., 2006; Xu et al., 2010, 2012;

125 Kowalewski et al., 2014). Mlynczak and Solomon (1991, 1993) and Mlynczak et al. (2013b) used  
126 the equilibrium assumption to derive exothermic chemical heat. The PEO assumption employed for  
127 studying the mesospheric OH\* layer response to gravity waves (Swenson and Gardner, 1998). In  
128 ultimately theoretical works, e.g. Grygalashvily et al. (2014), Grygalashvily (2015), PEO was used  
129 to derive the dependence of excited hydroxyl layer concentration and altitude on atomic oxygen  
130 and temperature. In the paper by Sonnemann et al. (2015) it was used to analyze annual variations  
131 of OH\* layer. Moreover, PEO is frequently applied implicitly, when authors are equating the night-  
132 time loss of ozone in the reaction with atomic hydrogen and production of ozone by a 3-body  
133 reaction of molecular and atomic oxygen (e.g., Nikoukar et al., 2007).

134 In the present Technical note we demonstrate how the photochemical equilibrium condition  
135 of several atmospheric components may be employed to statistically validate data of their  
136 simultaneous measurements, particularly in the case when measurement error is large.

137 We consider the simultaneous photochemical daytime equilibrium of OH, HO<sub>2</sub>, and O<sub>3</sub> at the  
138 altitudes of the mesosphere. We have derived a simplified algebraic equation

139  $F(OH, HO_2, O_3) = 1,$

140 describing the relationship between local concentrations of the components at the altitudes of 50–  
141 100 km. The only parameters of the equation are temperature, neutral density, local zenith angle,  
142 and constants of 8 reactions. One-year simulation of the mesosphere and lower thermosphere  
143 based on a 3D chemical-transport model shows that the discrepancy between the calculated  
144 evolution of the components and the equilibrium value given by the equation does not exceed 3–  
145 4 % in the full range of altitudes independent of season or latitude.

146 We have developed a technique of statistical Bayesian evaluation of simultaneous  
147 measurement of OH, HO<sub>2</sub> and O<sub>3</sub> based on the mentioned equilibrium equation taking into account  
148 the measurement error. The first results of its application to MLS/Aura data (Wang et al., 2015a,b;  
149 Schwartz et al., 2015) are presented. It is found that the satellite data of HO<sub>2</sub> distribution regularly  
150 demonstrates essentially lower altitudes of this component's mesospheric maximum. These results  
151 confirm the ones obtained via the offline retrieval of HO<sub>2</sub> from the MLS primary data (Millán et al.,  
152 2015).

153 The Technical Note is structured as follows. A 3D chemical transport model is briefly  
154 described in Sect. 2. In Sect. 3 a simplified algebraic relationship between the equilibrium  
155 concentrations of OH, HO<sub>2</sub> and O<sub>3</sub> is derived and verified by 3D simulations. Section 4 presents the

156 method of statistical evaluation of simultaneous data of OH, HO<sub>2</sub> and O<sub>3</sub>. The results of applying  
157 the method to MLS/Aura data are presented in Sect. 5. The last Section contains discussion of the  
158 results followed by concluding remarks.

159

## 160 **2. Model and calculations**

161

162 For our calculations we used the global 3D chemical transport model (CTM) of the middle  
163 atmosphere developed by the Leibniz Institute of Atmospheric Physics (IAP) (e.g., [Berger, 1994](#);  
164 [Ebel et al., 1995](#); [Sonnenmann et al., 1998](#); [Kremp et al., 1999](#); [Berger and von Zahn, 1999](#);  
165 [Hartogh et al., 2004, 2011](#); [Sonnenmann et al., 2006, 2007](#)). It was designed particularly for  
166 investigation of the spatio-temporal structure of phenomena in the MLT region and specifically in  
167 the extended mesopause region. The grid-point model extends from the ground up to the middle  
168 thermosphere (0–150 km; 118 pressure-height levels). The horizontal resolution amounts to 5.625°  
169 latitudinally and 5.625° longitudinally. The chemical module described in numerous papers (e.g.,  
170 [Sonnenmann et al., 1998](#); [Körner and Sonnenmann, 2001](#); [Grygalashvily et al., 2009, 2011, 2012](#))  
171 consists of 19 constituents, 49 chemical reactions, and 14 photo-dissociation reactions (see Table  
172 1). The reaction rates used in the model are taken from Burkholder et al. (2015). The temperature-  
173 dependent reaction rates are calculated on-line, thus, they are sensitive to small temperature  
174 fluctuations. We make use of the pre-calculated dissociation rates (Kremp et al., 1999).

175 The evolution of the components of HO<sub>x</sub> (H, OH, HO<sub>2</sub>, H<sub>2</sub>O<sub>2</sub>) and NO<sub>x</sub> (N, NO, NO<sub>2</sub>, NO<sub>3</sub>)  
176 families is calculated using the chemical family concept proposed by Shimazaki (Shimazaki, 1985).  
177 This is done because of the presence of short-lived components among these families, with  
178 lifetimes much shorter than those of the families themselves, which imposes significant restrictions  
179 on the value of the CTM's integration step. For example, the daytime lifetimes of OH and HO<sub>2</sub>  
180 above 70 km are about 1 s or less, while the lifetime of the HO<sub>x</sub> family is about 10<sup>4</sup> s or more.  
181 Therefore, when calculating these components individually it is necessary to set the CTM's  
182 integration step to be much less than 1 s. In our work, the Shimazaki technique is applied for  
183 calculating the evolution of each component of the HO<sub>x</sub> and NO<sub>x</sub> families. We emphasize that this  
184 technique does not explicitly use the steady-state approximation for the components, instead it  
185 utilizes the approach based on an implicit Euler scheme (see Shimazaki, 1985). This allows

186 increasing the integration step of CTM significantly without loss of accuracy of calculating the short-  
187 lived components. In our work the integration time is chosen to be 9 s.

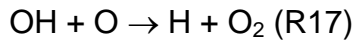
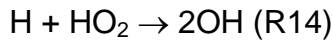
188 The model includes 3D advective and vertical diffusive transport (turbulent and molecular).  
189 Three-dimensional fields of temperature and winds are taken from the Canadian Middle  
190 Atmosphere Model (CMAM) for the year 2000 (de Grandpre et al., 2000; Scinocca et al., 2008).  
191 We use the Walcek-scheme (Walcek and Aleksic, 1998; Walcek, 2000) for advective transport and  
192 the implicit Thomas algorithm as described in Morton and Mayers (1994) for diffusive transport.  
193 The vertical eddy diffusion coefficient is based on the results by Lübken (1997).

194 ~~The CTM driven by COMMA-IAP middle atmosphere dynamics (Berger, 1994; Ebel et al.,  
195 Kremp et al., 1999; Berger and von Zahn, 1999) was verified by measurements, particularly  
196 for ozone, in a number of papers (Hartogh et al., 2004, 2011; Sonnemann et al., 2006, 2007).~~

197 We calculate the annual variation of spatio-temporal distributions of OH, HO<sub>2</sub>, and O<sub>3</sub> and  
198 constructed distributions of the  $F(OH, HO_2, O_3)$  function introduced in Sect. 1. To remove transitional  
199 regions that correspond to sunset and sunrise, we take into account only periods of local time with  
200 the solar zenith angle  $\chi < 85^\circ$ . The obtained results are presented in the model coordinates, so the  
201 pressure-height levels are used for the vertical axes. In addition, the approximate altitudes are  
202 shown in the figures of Sec. 1, calculated for a given month utilizing averaged temperature profiles  
203 of the model and hydrostatic equilibrium.

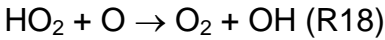
### 205 **3. Daytime photochemical equilibrium of OH, HO<sub>2</sub>, and O<sub>3</sub> at the altitudes of the mesosphere**

207 The daytime balance of OH concentration at mesospheric altitudes is determined by the following  
208 primary reactions (Brasseur and Solomon, 2005):

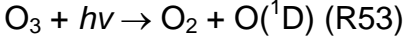
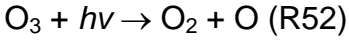
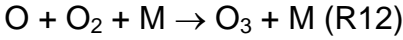


214 The daytime balance of HO<sub>2</sub> concentration:





218 The daytime balance of  $\text{O}_3$  concentration:



223 Expressions for local concentrations of  $\text{OH}$ ,  $\text{HO}_2$ , and  $\text{O}_3$  in the photochemical equilibrium  
224 are written in the form

$$225 \quad \text{OH} = \frac{k_{18} \cdot \text{HO}_2 \cdot \text{O} + 2k_{14} \cdot \text{HO}_2 \cdot \text{H} + k_{21} \cdot \text{O}_3 \cdot \text{H}}{k_{17} \cdot \text{O} + k_{22} \cdot \text{O}_3}, \quad (1)$$

$$226 \quad \text{HO}_2 = \frac{k_{20} \cdot \text{M} \cdot \text{O}_2 \cdot \text{H} + k_{22} \cdot \text{O}_3 \cdot \text{OH}}{k_{18} \cdot \text{O}}, \quad (2)$$

$$227 \quad \text{O}_3 = \frac{k_{12} \cdot \text{M} \cdot \text{O}_2 \cdot \text{O}}{k_{52} + k_{53} + k_{21} \cdot \text{H}}, \quad (3)$$

228 where  $k_i$  are the corresponding reaction constants from Burkholder et al. (2015).

229 We eliminate  $\text{O}$  and  $\text{H}$  from Eqs. (1)-(3) and derive an expression depending only on  $\text{OH}$ ,  $\text{HO}_2$ ,  $\text{O}_3$ .

230 Almost everywhere in the mesosphere and lower thermosphere (with the exception of 85-95  
231 km, see Kulikov et al., 2017) the photodissociation is the main ozone sink, i.e.  $k_{52} + k_{53} \gg k_{21} \cdot \text{H}$ .

232 Therefore, in the zero order approximation Eq. (3) can be simplified and the concentration of  
233 atomic oxygen can be defined in terms of ozone concentration:

$$234 \quad \text{O} = \frac{k_{52} + k_{53}}{k_{12} \cdot \text{M} \cdot \text{O}_2} \text{O}_3 \quad (4)$$

235 Making use of Eq. (4) we can derive from Eq. (2) an expression for the concentration of  $\text{H}$  in terms  
236 of concentrations of  $\text{OH}$ ,  $\text{HO}_2$  and  $\text{O}_3$ :

$$237 \quad \text{H} = \frac{k_{18} \cdot (k_{52} + k_{53}) / (k_{12} \cdot \text{M} \cdot \text{O}_2) \cdot \text{HO}_2 - k_{22} \cdot \text{OH}}{k_{20} \cdot \text{M} \cdot \text{O}_2} \text{O}_3 \quad (5)$$

238 By substituting this equation and Eq. (4) into Eq. (1) we obtain an expression relating  $\text{OH}$ ,  $\text{HO}_2$ , and  
239  $\text{O}_3$ :

$$240 \quad F(\text{OH}, \text{HO}_2, \text{O}_3) = \left( \frac{k_{20} \cdot \text{M} \cdot \text{O}_2}{k_{20} \cdot \text{M} \cdot \text{O}_2 + k_{21} \cdot \text{O}_3 + 2 \cdot k_{14} \cdot \text{HO}_2} + \frac{k_{12} \cdot \text{M} \cdot \text{O}_2 \cdot k_{22}}{(k_{52} + k_{53}) \cdot k_{17}} \right) \cdot \frac{k_{17} \cdot \text{OH}}{k_{18} \cdot \text{HO}_2} = 1 \quad (6)$$

241 Figure 1 shows height–latitude cross-sections of  $\langle F(OH, HO_2, O_3) \rangle$  for each month (in this

242 Section angle brackets denote monthly averaged zonal mean values). The dashed-gray area  
243 corresponds to  $\chi > 85^\circ$ . One can see that eq. (15) is most accurate within the 50–76 km range and  
244 above 86 km, where  $|\langle F \rangle - 1| \leq 1\%$ . The difference reaches 3–4 % in the region between 76 km  
245 and 86 km. The altitude of this region has an annual variation with a maximum deviation in the  
246 winter hemisphere. Below 50 km the value of  $\langle F \rangle$  increases up to 1.2 at 40 km, thus below the  
247 stratopause Eq. (6) no longer describes the simultaneous photochemical equilibrium of OH, HO<sub>2</sub>  
248 and O<sub>3</sub>. Note that these components remain short-lived below 50 km (with the lifetimes of about  
249 10<sup>2</sup>-10<sup>3</sup> s (Brasseur and Solomon, 2005)) depending on height and duration of daylight. However,  
250 for quantitative description of their daytime equilibrium it is necessary to include additional  
251 reactions involving, in particular, the components of the NO<sub>x</sub> family.

252 Note also that Eq. (1) and Eq. (6) take into account only the main daytime source of OH

253 ( $P_{OH}$ ) specified by reactions R18, R14, and R21:

$$254 P_{OH} = k_{18} \cdot HO_2 \cdot O + 2k_{14} \cdot HO_2 \cdot H + k_{21} \cdot O_3 \cdot H$$

255 These reactions run “inside” the HOx (H, OH, HO<sub>2</sub>, H<sub>2</sub>O<sub>2</sub>) family and do not perturb its total  
256 concentration. The height–latitude cross-sections of  $\langle P_{OH} \rangle$  for each month are presented in  
257 Fig. 2.

258 The next important daytime source of OH is specified by reactions R59 and R7 involving H<sub>2</sub>O, the  
259 main source for the HO<sub>x</sub> family:

$$260 P_{OH}^{H_2O} = (k_{59} + 2 \cdot k_7 \cdot O(^1D)) \cdot H_2O$$

261 Figure 3 shows height–latitude cross-sections of  $\langle P_{OH}^{H_2O} / P_{OH} \rangle$  for each month. Comparing Fig. 1  
262 and Fig. 3, we conclude that the previously indicated 3–4 % deviation of  $\langle F \rangle$  from 1 in the region  
263 between 76 km and 86 km is largely due to the neglect of these reactions.

264 Another source of OH is sporadically activated during charged particle precipitation events  
265 and exists for a relatively short time (several days). Solar proton events (SPE) perturb the ionic  
266 composition in the mesosphere and the upper stratosphere considerably and trigger a whole  
267 cascade of reactions involving ions, neutral components and their clusters (e.g., O<sub>2</sub><sup>+</sup>·H<sub>2</sub>O). This  
268 leads to an additional (to reactions R59 and R7) conversion of H<sub>2</sub>O molecules into OH and H  
269 (Solomon et al., 1981). The maximum of the OH production rate ( $P_{OH}^{SPE}$ ) induced by SPE is

located in the polar latitudes in the region of 60–80 km and, as a rule, does not exceed  $2 \cdot 10^3 \text{ cm}^{-3} \text{ s}^{-1}$  (Jackman et al., 2011, 2014). It can be seen from Fig. 2 that at these latitudes and altitudes the  $P_{OH}^{SPE} / P_{OH}$  ratio does not exceed 1-2%, even for the maximum values of  $P_{OH}^{SPE}$ . This means that the impact of  $P_{OH}^{SPE}$  on Eq. (6) is of the same order of smallness as in the case of reactions R59 and R7, hence, it may be neglected. A similar conclusion can be made for other reactions from Table 1, not accounted for by Eq. (6), including the ones involving  $\text{NO}_x$  in both quiet and perturbed conditions in the mesosphere.

#### 4. Method of statistical evaluation of simultaneous measurement of OH, $\text{HO}_2$ and $\text{O}_3$

The proposed method is based on the statistical Bayesian procedure described in the works by Kulikov et al. (2009) and Nechaev et al. (2016). It was originally developed for retrieving trace gas concentrations in the mesosphere from ground-based and satellite measurements of other mesospheric components. With respect to the considered evaluation problem this procedure consists of three steps: (1) constructing conditional probability density function (PDF) of OH,  $\text{HO}_2$  and  $\text{O}_3$  concentration values at each altitude  $z$  in the selected interval assuming that there is certain measurement data of these components and the algebraic relationship (6) is valid; (2) calculating the first moments of this distribution, i.e. expected value and dispersion of each component using the Metropolis-Hastings algorithm (Chib and Greenberg, 1995) for multidimensional integration; (3) comparing the obtained results with the initial measurement data.

For constructing posterior PDF it is convenient to introduce vector  $\bar{u}\{HO_2^{ret}, O_3^{ret}, OH^{ret}\}$ , whose components are the retrieved values of chemical species concentrations at a certain altitude  $z$ , and vector  $\bar{x}\{HO_2^m, O_3^m, OH^m\}$  composed of experimentally measured values of the components of vector  $\bar{u}$ ,  $x_j = u_j + \xi_j$ ,  $j = 1, 3$ , where  $\xi_j$  is a random error of measuring the  $j$ -th component of vector  $\bar{u}$  at the altitude  $z$ . It is assumed that

(1) random variables  $\xi_j$  are distributed normally with densities

$$w_j(\xi_j) = \frac{1}{\sigma_j \sqrt{2\pi}} \exp\left(-\frac{\xi_j^2}{2\sigma_j^2}\right); \quad (7)$$

(2)  $\xi_j$  are mutually independent:

298  $\vec{\xi} \{\xi_1, \xi_2, \xi_3\} \sim W_{\xi}(\vec{\xi}) = \prod_j w_j(\xi_j),$  (8)

299 where  $W_{\xi}(\vec{\xi})$  is the total PDF of all  $\xi_j$ ;

300 (3) dispersions  $\sigma_j$  in Eq. (7), that are expected error values, are assumed to be known a priori (in  
301 our case they are provided by the MLS retrieval algorithm along with measured data).

302 Then the probability to observe vector  $\vec{x}$  is given by the conditional PDF

303  $P_x(\vec{x} | \vec{u}) = \int \delta(\vec{x} - \vec{u}) W_{\xi}(\vec{\xi}') d^3 \vec{\xi}' = W_{\xi}(\vec{x} - \vec{u}),$  (9)

304 where  $\delta(\dots)$  is delta function.

305 The prior relationship of  $HO_2^{ret}$ ,  $O_3^{ret}$  and  $OH^{ret}$  concentrations (Eq. (6)) can be written as

306  $u_3 = G(u_1, u_2)$ . Integrating the left-hand side of Eq. (17) with conditional PDF of the variable  $u_3$ :

307  $P_{u_3}(u_3 | u_1, u_2) = \delta(u_3 - G(u_1, u_2)),$

308 yields a likelihood function of the model

309  $P_x(\vec{x} | u_1, u_2) = w_3(x_3 - G(u_1, u_2)) \cdot w_1(x_1 - u_1) w_2(x_2 - u_2).$  (10)

310 According to Bayes' theorem, the posterior function, i.e. the probability density of latent variables  $u_1$   
311 and  $u_2$ , under the condition that  $\vec{x}$  is observed, is defined by the expression

312 
$$P(u_1, u_2 | \vec{x}) \propto P_x(\vec{x} | u_1, u_2) \cdot P_{apr}(u_1, u_2) \\ \propto \exp\left(-\frac{(x_1 - u_1)^2}{2\sigma_1^2}\right) \cdot \exp\left(-\frac{(x_2 - u_2)^2}{2\sigma_2^2}\right) \cdot \exp\left(-\frac{(x_3 - G(u_1, u_2))^2}{2\sigma_3^2}\right) \cdot P_{apr}(u_1, u_2)$$
 (11)

313 in which  $P_{apr}(u_1, u_2)$  defines prior PDF of  $u_1$  and  $u_2$ .

314 The retrieved value of the latent variable  $u_{1,2,3}$  is hereinafter understood as the mean value  
315 of the function in Eq. (11):

316 
$$\langle u_{1,2} \rangle = \int_{-\infty}^{\infty} \int_{-\infty}^{\infty} u_{1,2} \cdot P(u_1, u_2 | \vec{x}) du_1 du_2$$
 (12)  

$$\langle u_3 \rangle = \int_{-\infty}^{\infty} \int_{-\infty}^{\infty} G(u_1, u_2) \cdot P(u_1, u_2 | \vec{x}) du_1 du_2.$$

317 Its dispersion defines the uncertainty of the retrieval:

318  $\sigma_{u_j} = \sqrt{\langle u_j^2 \rangle - \langle u_j \rangle^2}, \quad j = 1, 3,$  (13)

319 where the angle brackets denote averaging in the sense of Eq. (12).  
320

321 **5. MLS/Aura data evaluation and results**  
322

323 We used the latest version (v4.2) of the MLS “standard” product (Livesey et al., 2017) for trace gas  
324 concentrations and temperature  $T$  within the 1 – 0.046 mbar pressure interval where all data are  
325 suitable for scientific applications (Wang et al., 2015a,b; Schwartz et al., 2015). We took the  
326 daytime data when the solar zenith angle  $\chi < 80^\circ$  for January, May, and September 2005. All data  
327 were appropriately screened. “Pressure”, “estimated precision”, “status flag”, “quality”,  
328 “convergence” and “clouds” fields were taken into account.  $\text{HO}_2$  data were seen as the day-minus-  
329 night difference as prescribed by the MLS data guidelines (Livesey et al., 2017). Following Pickett  
330 et al. (2008), each daytime profile of this component measured on a given day at a latitude Lat, a  
331 profile resulting from averaging the nighttime profiles of  $\text{HO}_2$ , measured on the same day in the  
332 latitude range of  $\text{Lat} \pm 5^\circ$ , was subtracted. This operation eliminates systematic biases affecting  $\text{HO}_2$   
333 retrievals, but limits the studied latitude range to the one where MLS observes both daytime and  
334 nighttime data.

335 The integrals in Eq. (12)–(13) were calculated at every pressure level  $p$  for each set of  
336 simultaneously measured vertical profiles  $\text{OH}^{\text{MLS}}(p)$ ,  $\text{HO}_2^{\text{MLS}}(p)$ ,  $\text{O}_3^{\text{MLS}}(p)$ ,  $T^{\text{MLS}}(p)$ ,  $\sigma_{\text{OH}^{\text{MLS}}}(p)$ ,  
337  $\sigma_{\text{HO}_2^{\text{MLS}}}(p)$ ,  $\sigma_{\text{O}_3^{\text{MLS}}}(p)$ . The vertical profiles  $\langle \text{OH}^{\text{ret}} \rangle(p)$ ,  $\langle \text{HO}_2^{\text{ret}} \rangle(p)$ ,  $\langle \text{O}_3^{\text{ret}} \rangle(p)$ ,  $\sigma_{\text{OH}^{\text{ret}}}(p)$ ,  
338  $\sigma_{\text{HO}_2^{\text{ret}}}(p)$ ,  $\sigma_{\text{O}_3^{\text{ret}}}(p)$  were found at each point of the globe along the satellite track. Numerical  
339 integration was performed by a Monte Carlo method. For each pressure level, a sample of about  
340  $5 \cdot 10^5$  pairs of random variable values  $\{u_1, u_2\} = \{\text{HO}_2^{\text{ret}}, \text{O}_3^{\text{ret}}\}$  distributed with normalized probability  
341 density given by Eq. (11) with  $P_{\text{apr}}(u_1, u_2) \equiv 1$  was generated with the help of the Metropolis-  
342 Hastings algorithm (Chib and Greenberg, 1995). In this case, the statistical moments in Eq. (12)–  
343 (13) were determined by summation over the sample.

344 A typical example of retrieved profiles  $\text{HO}_2^{\text{ret}}$ ,  $\text{O}_3^{\text{ret}}$  and  $\text{OH}^{\text{ret}}$  (black curves) in comparison  
345 with the measured  $\text{HO}_2^{\text{MLS}}$ ,  $\text{O}_3^{\text{MLS}}$  and  $\text{OH}^{\text{MLS}}$  (red curves) is given in Fig. 4. First of all, note that  
346 statistics of the retrieved data is in satisfactory agreement with the initial measurement of OH and  
347  $\text{O}_3$  concentrations, but not of  $\text{HO}_2$ . The error of satellite measurement,  $\sigma_{\text{HO}_2^{\text{MLS}}}$ , greatly exceeds the

348 uncertainty of retrieval,  $\sigma_{HO_2^{ret}}$ , so at some altitudes the values of  $\langle HO_2^{MLS} \rangle$  (red dashed curves)  
 349 do not fall within the corresponding intervals  $\langle HO_2^{ret} \rangle \pm \sigma_{HO_2^{ret}}$ . Second, the results of a single  
 350 measurement of all three components and their retrieved values have considerable uncertainties  
 351 relative to their means within the whole interval of altitudes. Therefore, the observed and retrieved  
 352 data should be compared using the commonly accepted approach (e.g., Pickett et al., 2008) of  
 353 averaging large ensembles of profiles within certain latitude and time ranges, or zones. It is  
 354 supposed that the noise of satellite measurement instruments is delta-correlated, so that random  
 355 values corresponding to each single measured or retrieved profile are statistically independent. In  
 356 this case the dispersion of a measured or retrieved zonal mean profile is determined by summation

$$357 \quad \sigma_{\Sigma}^2 = \frac{1}{N^2} \sum_{k=1}^N \sigma_k^2,$$

358 where  $N$  is the number of measured or retrieved profiles within the zone and  $\sigma_k^2$  is the dispersion  
 359 of the  $k$ -th measured or retrieved profile.

360 The range of latitudes covered by the satellite trajectory was divided into 17 bins  $10^0$  each.  
 361 About 3000 single profiles of each chemical component fall into one bin during a month of  
 362 MLS/Aura observations. Therefore, the resulting uncertainties due to measurement noise of OH,  
 363  $HO_2$  and  $O_3$  concentration profiles (both measured and retrieved) averaged over such ensembles  
 364 are significantly (about one and a half order of magnitude) lower than the uncertainties of individual  
 365 profiles. Examples of such profiles for January, May and September 2005 are presented in Fig. 5.  
 366 One can see that the indicated uncertainties are now small enough to make clear conclusions  
 367 about the extent to which the observed and retrieved profiles agree by comparing their averaged  
 368 values only, i.e.  $\langle OH^{MLS} \rangle$ ,  $\langle HO_2^{MLS} \rangle$ ,  $\langle O_3^{MLS} \rangle$  and  $\langle OH^{ret} \rangle$ ,  $\langle HO_2^{ret} \rangle$ ,  $\langle O_3^{ret} \rangle$ .

369 Figures 4–6 show monthly averaged zonal mean pressure–latitude cross-sections of  
 370  $\langle HO_2^{ret} \rangle$ ,  $\langle HO_2^{MLS} \rangle$ ,  $\Delta HO_2 = (\langle HO_2^{ret} \rangle - \langle HO_2^{MLS} \rangle) / \langle HO_2^{MLS} \rangle$  and similar characteristics  
 371 for OH and  $O_3$  concentration profiles for three months of the year 2005. First, clearly, the  
 372 distributions of  $\langle OH^{ret} \rangle$  and  $\langle O_3^{ret} \rangle$  are in good qualitative and quantitative agreement with the  
 373 initial MLS/Aura measurement data at lower altitudes, below  $\sim 0.07$  mbar and 0.1 mbar,  
 374 correspondingly. At higher altitudes, the distributions of  $\langle OH^{ret} \rangle$  reproduce all the main structural  
 375 features of  $\langle OH^{MLS} \rangle$ , but the retrieved OH concentration has lower values than the observed one

376 with a relative difference  $\Delta OH$  reaching  $\sim 15\%$  at the top. The distribution of  $\langle O_3^{ret} \rangle$  above  
377 0.1 mbar, in turn, differs considerably from  $\langle O_3^{MLS} \rangle$ , both in quantity and quality, and  $\Delta O_3$  locally  
378 reaches 50-60% and more. Second, for all months there are significant qualitative and quantitative  
379 differences between  $\langle HO_2^{ret} \rangle$  and  $\langle HO_2^{MLS} \rangle$ , the most noticeable one being location of the  
380 mesospheric maximum of this component's concentration. According to the observations it is close  
381 to 0.1 mbar, while the retrieved data demonstrate the altitudes of about  $\sim 0.046$  mbar or higher. Our  
382 analysis of the applied method of statistical evaluation demonstrates that the higher position of this  
383 maximum in the distributions of  $\langle HO_2^{ret} \rangle$  is influenced by the  $OH^{MLS}$  data in which the  
384 mesospheric maximum (see Figs. 6-8) is also located notably higher than 0.1 mbar.

385

## 386 **6. Discussion and conclusion**

387

388 On the basis of the data presented in Section 5 we can conclude that, upon the whole,  
389 simultaneous OH,  $HO_2$  and  $O_3$  satellite measurements poorly satisfy the photochemical equilibrium  
390 condition. The  $HO_2$  component biases from this condition most prominently. We can conjecture that  
391 a possible explanation for the bias is the significant systematic error in  $HO_2$  measurements, in  
392 particular, in the height of the mesospheric maximum. This assumption is supported by the  
393 calculation of the  $HO_2$  distributions with the use of our 3D chemical transport model (see Fig. 9). It  
394 can be seen that the mesospheric maximum of  $HO_2$  in these months, as well as of the  $\langle HO_2^{ret} \rangle$   
395 distributions, lies above 0.046 mbar.

396 Moreover, new data on the  $HO_2$  distributions were recently obtained from the MLS  
397 measurements. Millán et al. (2015) performed the offline retrieval of daily zonal means of  $HO_2$   
398 profiles using averaged MLS radiances measured in  $10^\circ$  latitude bins. Averaged spectra have a  
399 better signal to noise ratio, which removes many of the limitations of the MLS standard product for  
400  $HO_2$ . In particular, the upper boundary of the altitude region in which daytime data is suitable for  
401 scientific use has reached 0.0032 mbar, and the "day-minus-night" correction is not needed at  
402 altitudes above 1 mbar. Comparison with various experimental and model data has shown that the  
403 offline retrieval reproduces the basic properties of the  $HO_2$  distribution in the mesosphere relatively  
404 well (at least qualitatively) (Millán et al. 2015).

405 The offline retrieval product, the alternative dataset of daytime  $HO_2$ , has recently become

406 publicly available at <https://mls.jpl.nasa.gov>. Figure 10 shows the monthly averaged zonal means  
 407 of offline retrieval data ( $\langle HO_2^{MLS}_{offline} \rangle$ ) and relative differences with retrieved and MLS standard  
 408 product data  $(\langle HO_2^{MLS} \rangle - \langle HO_2^{MLS}_{offline} \rangle) / \langle HO_2^{MLS}_{offline} \rangle$  and  
 409  $(\langle HO_2^{ret} \rangle - \langle HO_2^{MLS}_{offline} \rangle) / \langle HO_2^{MLS}_{offline} \rangle$ , correspondingly. Figure 10 represents the same time  
 410 periods as Figs. 6-8. It is worth noting that the distributions  $\langle HO_2^{MLS}_{offline} \rangle$  depicted in Fig. 10  
 411 represent significantly different amounts of data. The data sets for May and September include 31  
 412 and 27 days of measurements, respectively, whereas the January dataset encompasses only 4  
 413 days. The latter makes the graphs in the first row in Fig. 10 noisier than the others. One can see  
 414 that the results of the offline  $HO_2$  retrieval show the same features as the results of our evaluation  
 415 technique in comparison to the standard MLS retrieval, i.e. the height of mesospheric  $HO_2$   
 416 maximum is notably higher. We can conclude that the distributions of  $\langle HO_2^{ret} \rangle$  better match  
 417  $\langle HO_2^{MLS}_{offline} \rangle$  than  $\langle HO_2^{MLS} \rangle$ , although some quantitative discrepancy between  $\langle HO_2^{ret} \rangle$  and  
 418  $\langle HO_2^{MLS}_{offline} \rangle$  also exists. Note that this may be due to systematic errors in the  $HO_2^{MLS}$   
 419 distributions, which cannot be excluded within the framework of the introduced technique. For a  
 420 detailed qualitative and quantitative comparison of  $\langle HO_2^{ret} \rangle$  and  $\langle HO_2^{MLS}_{offline} \rangle$  one should  
 421 modify the method, so that a statistical evaluation of the  $OH^{MLS}$  and  $O_3^{MLS}$  standard products, and  
 422 the data of the offline  $HO_2$  retrieval could be conducted within the framework of a single procedure  
 423 with no account for the  $HO_2^{MLS}$  distributions. This modification is under way and will be presented  
 424 elsewhere.

425 The proposed method for statistical evaluation of mesospheric species measurements can  
 426 be readily generalized to other atmospheric photochemical systems that contain short-lived  
 427 components (see Introduction). It may also be modified for assessing hard to measure chemical  
 428 components, characteristics of atmospheric processes (like wind speed or turbulent diffusion rate),  
 429 or poorly known reaction rates.

430

431 **Acknowledgments**

432 The work was carried out within the framework of the state assignment of IAP RAS (project 0035-  
 433 2014-0033) This work and was supported partially by the Russian Foundation for Basic Research  
 434 (project №17-05-01142) Science Foundation (contract № 15-17-10024 of June 04, 2015). The

435 data used in this study is supported by the Institute of Applied Physics of the Russian Academy of  
436 Sciences (Nizhny Novgorod, Russia). Inquiries about the distributions used in this paper can be  
437 addressed to Mr. Belikovich (belikovich@ipfran.ru).

438

## 439 References

440

441 Avallone, L. M., and Toohey, D. W.: Tests of halogen photochemistry using in situ  
442 measurements of ClO and BrO in the lower polar stratosphere, *J. Geophys. Res.*, Volume 106,  
443 Issue D10, Pages 10411–1042, doi: 10.1029/2000JD900831, 2001.

444 Benton, A. K., Langridge, J. M., Ball, S. M., Bloss, W. J., Dall'Osto, M., Nemitz, E., Harrison,  
445 R. M., and Jones, R. L.: Night-time chemistry above London: measurements of NO<sub>3</sub> and N<sub>2</sub>O<sub>5</sub>  
446 from the BT Tower, *Atmos. Chem. Phys.*, 10, 9781-9795, doi:10.5194/acp-10-9781-2010, 2010.

447 Berger, U.: Numerische Simulation klimatologischer Prozesse und thermische Gezeiten in  
448 der mittleren Atmosphä~~re~~, Thesis, Univ. Cologne, Germany, 1994.

449 Berger, U. and von Zahn, U.: The two-level structure of the mesopause: A model study, *J.*  
450 *Geophys. Res.*, 104, 22083–22093, 1999.

451 Berthet, G., Ricaud, P., Lefevre, F., Le Flochmoen, E., Urban, J., Barret, B., Lautie, N.,  
452 Dupuy, E., De La Noe, J., and Murtagh, D.: Nighttime chlorine monoxide observations by the Odin  
453 satellite and implications for the ClO/Cl<sub>2</sub>O<sub>2</sub> equilibrium, *Geophys. Res. Lett.*, 32, L11812,  
454 doi:10.1029/2005GL022649, 2005.

455 Brasseur, G. and Solomon, S.: Aeronomy of the Middle Atmosphere, 644 pp., 3rd edition,  
456 Springer, The Netherlands, 2005.

457 Brown, S. S., Stark, H., Ryerson, T. B., Williams, E. J., Nicks Jr., D. K., Trainer, M.,  
458 Fehsenfeld, F. C., and Ravishankara, A. R.: Nitrogen oxides in the nocturnal boundary layer:  
459 Simultaneous in situ measurements of NO<sub>3</sub>, N<sub>2</sub>O<sub>5</sub>, NO<sub>2</sub>, NO, and O<sub>3</sub>, *J. Geophys. Res.*, 108(D9),  
460 4299, doi:10.1029/2002JD002917, 2003.

461 Burkholder, J. B., S. P. Sander, J. Abbatt, J. R. Barker, R. E. Huie, C. E. Kolb, M. J. Kurylo,  
462 V. L. Orkin, D. M. Wilmouth, and P. H. Wine [\(2015\)](#), Chemical Kinetics and Photochemical Data for  
463 Use in Atmospheric Studies, Evaluation No. 18, JPL Publication 15-10, Jet Propulsion Laboratory,  
464 Pasadena, <http://jpldataeval.jpl.nasa.gov> [\(2015\)](#).

465 Butz, A., H. Bosch, C. Camy-Peyret, M. Dorf, A. Engel, S. Payan, and Pfeilsticker, K.:  
466 Observational constraints on the kinetics of the ClO-BrO and ClO-ClO ozone loss cycles in the  
467 Arcticwinter stratosphere, *Geophys. Res. Lett.*, 34, L05801, doi:10.1029/2006GL028718, 2007.

468 Cantrell, C. A., Mauldin, L., Zondlo, M., Eisele, F., Kosciuch, E., Shetter, R., Lefer, B., Hall,  
469 S., Campos, T., Ridley, B., Walega, J., Fried, A., Wert, B., Flocke, F., Weinheimer, A., Hannigan,  
470 J., Coffey, M., Atlas, E., Stephens, S., Heikes, B., Snow, J., Blake, D., Blake, N., Katzenstein, A.,  
471 Lopez, J., Browell, E. V., Dibb, J., Scheuer, E., Seid, G., and Talbot, R.: Steady state free radical  
472 budgets and ozone photochemistry during TOPSE, *J. Geophys. Res.*, 108(D4), 8361,  
473 doi:10.1029/2002JD002198, 2003.

474 Chameides, W.: Tropospheric odd nitrogen and the atmospheric water vapor cycle, *J.  
475 Geophys. Res.*, 84 (C10), 4989–4996, doi: 10.1029/JC080i036p04989, 1975.

476 Chib, S., and Greenberg, E.: Understanding the Metropolis-Hastings Algorithm, *The  
477 American Statistician*, 49 (4), 327-335, doi: 10.2307/2684568, 1995.

478 Crawford, J., Davis, D., Chen, G., Bradshaw, J., Sandholm, S., Gregory, G., Sachse, G.,  
479 Anderson, B., Collins, J., Blake, D., Singh, H., Heikes, B., Talbot, R., Rodriguez, J.: Photostationary  
480 state analysis of the NO<sub>2</sub>-NO system based on airborne observations from the western and central  
481 North Pacific, 101(D1), 2053–2072, doi: 10.1029/95JD02201, 1996.

482 Crowley, J. N., Schuster, G., Pouvesle, N., Parchatka, U., Fischer, H., Bonn, B., Bingemer,  
483 H., and Lelieveld, J.: Nocturnal nitrogen oxides at a rural mountain-site in south-western Germany,  
484 *Atmos. Chem. Phys.*, 10, 2795-2812, doi:10.5194/acp-10-2795-2010, 2010.

485 de Grandpre, J., Beagley, S. R., Fomichev, V. I., Griffioen, E., McConnell, J. C., Medvedev,  
486 A. S., and Shepherd, T. G.: Ozone climatology using interactive chemistry: Results from the  
487 Canadian Middle Atmosphere Model, *J. Geophys. Res.-Atmos.*, 105, 26475-26491,  
488 doi:10.1029/2000JD900427, 2000.

489 Djouad, R., Michelangeli, D. V., and Gong, W.: Numerical solution for atmospheric  
490 multiphase models: Testing the validity of equilibrium assumptions, *J. Geophys. Res.*, 108(D19),  
491 4602, doi:10.1029/2002JD002969, 2003.

492 Douglass, A. R., Jackman, C. H., and Stolarski, R. S.: Comparison of model results  
493 transporting the odd nitrogen family with results transporting separate odd nitrogen species, *J.  
494 Geophys. Res.*, 94(D7), 9862–9872, doi:10.1029/JD094iD07p09862, 1989.

495 Ebel, A., Berger, U., and Krueger, B. C.: Numerical simulations with COMMA, a global  
496 model of the middle atmosphere, SIMPO Newsletter, 12, 22–32, 1995.

497 Evans, W. F. J., and Llewellyn, E. J.: Atomic hydrogen concentrations in the mesosphere  
498 and the hydroxyl emissions, *J. Geophys. Res.*, 78, 323–326, doi:10.1029/JA078i001p00323, 1973.

499 | Evans, W. F. J., McDade, I. C., Yuen, J., and Llewellyn, E. J.: A rocket measurement of the  
500 O<sub>2</sub> infrared atmospheric (0-0) band emission in the dayglow and a determination of the  
501 mesospheric ozone and atomic oxygen densities, *Can. J. Phys.*, 66, 941–946, doi:10.1139/p88-15,  
502 1988.

503 Feigin, A. M., and Konovalov, I. B.: On the possibility of complicated dynamic behavior of  
504 atmospheric photochemical systems: Instability of the Antarctic photochemistry during the ozone  
505 hole formation, *J. Geophys. Res.*, 101, 26023–26038, doi:10.1029/96JD02011, 1996.

506 Feigin, A. M., Konovalov, I. B., and Molkov, Ya. I.: Towards understanding nonlinear nature  
507 of atmospheric photochemistry: Essential dynamic model of the mesospheric photochemical  
508 system, *J. Geophys. Res.*, 103, 25447–25460, doi:10.1029/98JD01569, 1998.

509 Funke, B., Lopez-Puertas, M., von Clarmann, T., Stiller, G. P., Fischer, H., Glatthor, N.,  
510 Grabowski, U., Hopfner, M., Kellmann, S., Kiefer, M., Linden, A., Mengistu Tsidu, G., Milz, M.,  
511 Steck, T. and Wang, D. Y.: Retrieval of stratospheric NO<sub>x</sub> from 5.3 and 6.2 mm nonlocal  
512 thermodynamic equilibrium emissions measured by Michelson Interferometer for Passive  
513 Atmospheric Sounding (MIPAS) on Envisat, *J. Geophys. Res.*, 110, D09302,  
514 doi:10.1029/2004JD005225, 2005.

515 Ghosh, S., Pyle, J. A., and Good, P.: Temperature dependence of the ClO concentration  
516 near the stratopause, *J. Geophys. Res.*, 102(D15), 19207–19216, doi:10.1029/97JD01099, 1997.

517 Good, R. E.: Determination of atomic oxygen density from rocket borne measurements of  
518 hydroxyl airglow, *Planet. Space Sci.*, 24, 389–395, doi.org/10.1016/0032-0633(76)90052-0, 1976.

519 Grygalashvily, M., Sonnemann, G. R., and Hartogh, P.: Long-term behavior of the  
520 concentration of the minor constituents in the mesosphere—A model study, *Atmos. Chem. Phys.*,  
521 9, 2779–2792, doi:10.5194/acp-9-2779-2009, 2009.

522 Grygalashvily, M., Becker, E., and Sonnemann, G. R.: Wave mixing effects on minor  
523 chemical constituents in the MLT region: Results from a global CTM driven by high-resolution  
524 dynamics, *J. Geophys. Res.*, 116, D18302, doi:10.1029/2010JD015518, 2011.

525 Grygalashvly, M., Becker, E., and Sonnemann, G. R.: Gravity wave mixing and effective  
526 diffusivity for minor chemical constituents in the mesosphere/lower thermosphere, *Space Sci. Rev.*,  
527 168, 333–362, doi:10.1007/s11214-011-9857-x, 2012.

528 Grygalashvly, M., Sonnemann, G. R., Lübken, F.-J., Hartogh, P., and Berger, U.: Hydroxyl  
529 layer: Mean state and trends at midlatitudes, *J. Geophys. Res.-Atmos.*, 119, 12391–12419,  
530 doi:10.1002/2014JD022094, 2014.

531 Grygalashvly, M.: Several notes on the OH\* layer, *Ann. Geophys.*, 33, 923-930,  
532 doi:10.5194/angeo-33-923-2015, 2015.

533 Hartogh, P., Jarchow, C., Sonnemann, G. R., and Grygalashvly, M.: On the spatiotemporal  
534 behavior of ozone within the upper mesosphere/mesopause region under nearly polar night  
535 conditions, *J. Geophys. Res.*, 109, D18303, doi:10.1029/2004JD004576, 2004.

536 Hartogh, P., Sonnemann, G. R., Grygalashvly, M., and Jarchow, Ch.: Ozone trends in mid-  
537 latitude stratopause region based on microwave measurements at Lindau (51.66° N, 10.13° E), the  
538 ozone reference model, and model calculations, *Adv. Space Res.*, 47, 1937-1948,  
539 doi:10.1016/j.asr.2011.01.010, 2011.

540 Hauchecorne, A., Bertaux, J. L., Dalaudier, F., Keckhut, P., Lemennais, P., Bekki, S.,  
541 Marchand, M., Lebrun, J. C., Kyrölä, E., Tamminen, J., Sofieva, V., Fussen, D., Vanhellemont, F.,  
542 Fanton d'Andon, O., Barrot, G., Blanot, L., Fehr, T., and Saavedra de Miguel, L.: Response of  
543 tropical stratospheric O<sub>3</sub>, NO<sub>2</sub> and NO<sub>3</sub> to the equatorial Quasi-Biennial Oscillation and to  
544 temperature as seen from GOMOS/ENVISAT, *Atmos. Chem. Phys.*, 10, 8873-8879,  
545 doi:10.5194/acp-10-8873-2010, 2010.

546 Jackman, C. H., Marsh, D. R., Vitt, F. M., Roble, R. G., Randall, C. E., Bernath, P. F., Funke,  
547 B., López-Puertas, M., Versick, S., Stiller, G. P., Tylka, A. J., and Fleming, E. L.: Northern  
548 Hemisphere atmospheric influence of the solar proton events and ground level enhancement in  
549 January 2005, *Atmos. Chem. Phys.*, 11, 6153-6166, <https://doi.org/10.5194/acp-11-6153-2011>,  
550 2011.

551 Jackman, C. H., Randall, C. E., Harvey, V. L., Wang, S., Fleming, E. L., López-Puertas, M.,  
552 Funke, B., and Bernath, P. F.: Middle atmospheric changes caused by the January and March  
553 2012 solar proton events, *Atmos. Chem. Phys.*, 14, 1025-1038, <https://doi.org/10.5194/acp-14-1025-2014>, 2014.

555 Kawa, S. R., Fahey, D. W., Solomon, S., Brune, W. H., Proffitt, M. H., Toohey, D. W.,  
556 Anderson Jr., D. E., Anderson, L. C., and Chan, K. R.: Interpretation of aircraft measurements of  
557 NO, ClO, and O<sub>3</sub> in the lower stratosphere, *J. Geophys. Res.*, 95(D11), 18597–18609 doi:  
558 10.1029/JD095iD11p18597, 1990.

559 Kremp, C., Berger, U., Hoffmann, P., Keuer, D., and Sonnemann, G. R.: Seasonal variation  
560 of middle latitude wind fields of the mesopause region – a comparison between observation and  
561 model calculation, *Geophys. Res. Lett.*, 26, 1279–1282, 1999.

562 Kaye, J. A., and Rood, R. B.: Chemistry and transport in a three-dimensional stratospheric  
563 model: Chlorine species during a simulated stratospheric warming, *J. Geophys. Res.*, 94(D1),  
564 1057–1083, doi: 10.1029/JD094iD01p01057, 1989.

565 Ko, M., Hu, W., Rodriguez, J. M., Kondo, Y., Koike, M., Kita, K., Kawakami, S., Blake, D.,  
566 Liu, S., and Ogawa, T.: Photochemical ozone budget during the BIBLE A and B campaigns, *J.*  
567 *Geophys. Res.*, 107, 8404, doi:10.1029/2001JD000800, 2002. [printed 108(D3), 2003].

568 Kondo, Y., Matthews, W. A., Aimedieu, P., and Robbins, D. E. Diurnal variation of nitric  
569 oxide at 32 km: Measurements and interpretation, *J. Geophys. Res.*, 93(D3), 2451–2460,  
570 doi:10.1029/JD093iD03p02451, 1988.

571 Kondo, Y., Ziereis, H., Koike, M., Kawakami, S., Gregory, G. L., Sachse, G. W., Singh, H.  
572 B., Davis, D. D., Merrill, J. T.: Reactive nitrogen over the Pacific Ocean during PEM-West, A  
573 101(D1), 1809–1828, doi:10.1029/95JD02611, 1996.

574 Konovalov, I. B., Feigin, A. M., Mukhina, A. Y.: Toward understanding of the nonlinear  
575 nature of atmospheric photochemistry: Multiple equilibrium states in the high-latitude lower  
576 stratospheric photochemical system, *J. Geophys. Res.*, 104, 8669–8689,  
577 doi:10.1029/1998JD100037, 1999.

578 Konovalov, I. B., and Feigin, A. M.: Toward an understanding of the nonlinear nature of  
579 atmospheric photochemistry: Origin of the complicated dynamic behaviour of the mesospheric  
580 photochemical system, *Nonlin. Processes Geophys.*, 7, 87–104, doi:10.5194/npg-7-87-2000, 2000.

581 Körner, U., and Sonnemann, G. R.: Global 3D-modeling of water vapor concentration of the  
582 mesosphere/mesopause region and implications with respect to the NLC region, *J. Geophys. Res.-*  
583 *Atmos.*, 106, 9639–9651, doi:10.1029/2000JD900744, 2001.

584 Kowalewski, S., von Savigny, C., Palm, M., McDade, I. C., and Notholt, J.: On the impact of  
585 the temporal variability of the collisional quenching process on the mesospheric OH emission layer:

586 a study based on SD-WACCM4 and SABER, *Atmos. Chem. Phys.*, 14, 10193-10210,  
587 doi:10.5194/acp-14-10193-2014, 2014.

588 Kremser, S., Schofield, R., Bodeker, G. E., Connor, B. J., Rex, M., Barret, J., Mooney, T.,  
589 Salawitch, R. J., Carty, T., Frier, K., Chipperfield, M. P., Langematz, U., and Feng, W.: Retrievals  
590 of chlorine chemistry kinetic parameters from Antarctic ClO microwave radiometer measurements,  
591 *Atmos. Chem. Phys.*, 11, 5183-5193, doi:10.5194/acp-11-5183-2011, 2011.

592 Kulikov, M. Y., Feigin, A. M., and Sonnemann, G. R.: Retrieval of the vertical distribution of  
593 chemical components in the mesosphere from simultaneous measurements of ozone and hydroxyl  
594 distributions, *Radiophys. Quantum Electron.*, 49, 683-691, doi:10.1007/s11141-006-0103-4, 2006.

595 Kulikov, M. Yu., Feigin, A. M., and Sonnemann, G. R.: Retrieval of water vapor profile in the  
596 mesosphere from satellite ozone and hydroxyl measurements by the basic dynamic model of  
597 mesospheric photochemical system, *Atmos. Chem. Phys.*, 9, 8199-8210, doi:10.5194/acp-9-8199-  
598 2009, 2009.

599 Kulikov, M. Y., Mukhin, D. N., and Feigin, A. M.: Bayesian strategy of accuracy estimation  
600 for characteristics retrieved from experimental data using base dynamic models of atmospheric  
601 photochemical systems, *Radiophys. Quantum Electron.*, 52, 618-626, doi:10.1007/s11141-010-  
602 9171-6, 2009.

603 Kulikov, M. Yu., Vadimova, O. L., Ignatov, S. K., and Feigin, A. M.: The mechanism of non-  
604 linear photochemical oscillations in the mesopause region, *Nonlinear Processes in Geophysics*,  
605 v.19, p.p.501-512, doi:10.5194/npg-19-501-2012, 2012.

606 Kulikov, M. Yu., and Feigin, A. M.: Automated construction of the basic dynamic models of  
607 the atmospheric photochemical systems using the RADM2 chemical mechanism as an example,  
608 *Radiophys. Quantum Electron.*, 57, 478-487, doi 10.1007/s11141-014-9530-9, 2014.

609 Kulikov, M. Y., Belikovich, M. V., Grygalashvily, M., Sonnemann, G. R., Ermakova, T. S.,  
610 Nechaev, A. A., and Feigin, A. M.: Daytime ozone loss term in the mesopause region, *Ann.*  
611 *Geophys.*, 35, 677-682, doi:10.5194/angeo-35-677-2017, 2017.

612 Livesey, N. J., Read, W. G., Wagner, P. A., Froideau, L., Lambert, A., Manney, G. L.,  
613 Millan, L. F., Pumphrey, H. C., Santee, M. L., Schwartz, M. J., Wang, S., Fuller, R. A., Jarnot, R. F.,  
614 Knosp, B. W., and Martinez E.: Earth Observing System (EOS) Aura Microwave Limb Sounder  
615 (MLS) Version 4.2 Level 2 data quality and description document, JPL D-33509, JPL publication,  
616 USA, 2017.

617 Llewellyn, E. J., McDade, I. C., Moorhouse, P., and Lockerbie, M. D.: Possible reference  
618 models for atomic oxygen in the terrestrial atmosphere, *Adv. Space Res.*, 13, 135–144,  
619 doi:10.1016/0273-1177(93)90013-2, 1993.

620 Llewellyn, E. J., and McDade, I. C.: A reference model for atomic oxygen in the terrestrial  
621 atmosphere, *Adv. Space Res.*, 18, 209–226, doi:10.1016/0273-1177(96)00059-2, 1996.

622 Luübken, F. J.: Seasonal variation of turbulent energy dissipation rates at high latitudes as  
623 determined by in situ measurements of neutral density fluctuations, *J. Geophys. Res.*, 102, 13441–  
624 13456, 1997.

625 Marchand, M., Bekki, S., Lefevre, F., and Hauchecorne, A.: Temperature retrieval from  
626 stratospheric O<sub>3</sub> and NO<sub>3</sub> GOMOS data, *Geophys. Res. Lett.*, 34, L24809,  
627 doi:10.1029/2007GL030280, 2007.

628 Marsh, D. R., Smith, A. K., Mlynczak, M. G., and Russell III, J. M.: SABER observations of  
629 the OH Meinel airglow variability near the mesopause, *J. Geophys. Res.*, 111, A10S05,  
630 doi:10.1029/2005JA011451, 2006.

631 Martinez, M., Perner, D., Hackenthal, E.-M., Kulzer, S., and Schultz, L.: NO<sub>3</sub> at Helgoland  
632 during the NORDEX campaign in October 1996, *J. Geophys. Res.*, 105(D18), 22,685–22,695,  
633 doi:10.1029/2000JD900255, 2000.

634 Massie, S. T., and Hunten, D. M.: Stratospheric eddy diffusion coefficients from tracer data,  
635 *J. Geophys. Res.*, 86(C10), 9859–9868, doi:10.1029/JC086iC10p09859, 1981.

636 McDade, I. C., Llewellyn, E. J., and Harris, F. R.: Atomic oxygen concentrations in the lower  
637 auroral thermosphere, *Adv. Space Res.*, 5(7), 229–232, doi:10.1016/0273-1177(85)90379-5, 1985.

638 McDade, I. C., and Llewellyn, E. J.: Mesospheric oxygen atom densities inferred from  
639 night-time OH Meinel band emission rates, *Planet. Space Sci.*, 36, 897–905, DOI:10.1016/0032-  
640 0633(88)90097-9, 1988.

641 McLaren, R., Wojtal, P., Majonis, D., McCourt, J., Halla, J. D., and Brook, J.: NO<sub>3</sub> radical  
642 measurements in a polluted marine environment: links to ozone formation, *Atmos. Chem. Phys.*,  
643 10, 4187–4206, doi:10.5194/acp-10-4187-2010, 2010.

644 Millán, L., Wang, S., Livesey, N., Kinnison, D., Sagawa, H., and Kasai, Y.: Stratospheric and  
645 mesospheric HO<sub>2</sub> observations from the Aura Microwave Limb Sounder, *Atmos. Chem. Phys.*, 15,  
646 2889–2902, doi:10.5194/acp-15-2889-2015, 2015.

647 Mlynczak, M. G., and Solomon, S.: Middle atmosphere heating by exothermic chemical  
648 reactions involving odd-hydrogen species, *Geophys. Res. Lett.*, 18, 37-40,  
649 doi:10.1029/90GL02672, 1991.

650 Mlynczak, M. G., and Solomon, S.: A detailed evaluation of the heating efficiency in the  
651 middle atmosphere, *J. Geophys. Res.*, 98, 10,517–10,541, doi:10.1029/93JD00315, 1993.

652 Mlynczak, M. G., Marshall, B. T., Martin-Torres, F. J., Russell III, J. M., Thompson, R. E.,  
653 Remsberg, E. E., and Gordley, L. L.: Sounding of the Atmosphere using Broadband Emission  
654 Radiometry observations of daytime mesospheric O<sub>2</sub>(1D) 1.27  $\mu$ m emission and derivation of  
655 ozone, atomic oxygen, and solar and chemical energy deposition rates, *J. Geophys. Res.*, 112,  
656 D15306, doi:10.1029/2006JD008355, 2007.

657 Mlynczak, M. G., Hunt, L. A., Mast, J. C., Marshall, B. T., Russell III, J. M., Smith, A. K.,  
658 Siskind, D. E., Yee, J.-H., Mertens, C. J., Martin-Torres, F. J., Thompson, R. E., Drob, D. P., and  
659 Gordley, L. L.: Atomic oxygen in the mesosphere and lower thermosphere derived from SABER:  
660 Algorithm theoretical basis and measurement uncertainty, *J. Geophys. Res.*, 118, 5724–5735,  
661 doi:10.1002/jgrd.50401, 2013a.

662 Mlynczak, M. G., Hunt, L. H., Mertens, C. J., Marshall, B. T., Russell III, J. M., López-  
663 Puertas, M., Smith, A. K., Siskind, D. E., Mast, J. C., Thompson, R. E., and Gordley, L. L.:  
664 Radiative and energetic constraints on the global annual mean atomic oxygen concentration in the  
665 mesopause region, *J. Geophys. Res. Atmos.*, 118, 5796–5802, doi:10.1002/jgrd.50400, 2013b.

666 Mlynczak, M. G., Hunt, L. A., Marshall, B. T., Mertens, C. J., Marsh, D. R., Smith, A. K.,  
667 Russell, J. M., Siskind, D. E., and Gordley, L. L.: Atomic hydrogen in the mesopause region  
668 derived from SABER: Algorithm theoretical basis, measurement uncertainty, and results, *J.*  
669 *Geophys. Res.*, 119, 3516–3526, doi:10.1002/2013JD021263, 2014.

670 Morton, K. W., and D. F. Mayers, *Numerical Solution of Partial Differential Equations*,  
671 Cambridge University Press, 1994.

672 Nechaev, A. A., Ermakova, T. S., and Kulikov, M. Y.: Determination of the Trace-Gas  
673 Concentrations at the Altitudes of the Lower and Middle Mesosphere from the Time Series of  
674 Ozone Concentration, *Radiophys. Quantum Electron.*, 59, 546–559, doi:10.1007/s11141-016-  
675 9722-6, 2016.

676 Nikoukar, R., Swenson, G. R., Liu, A. Z., and Kamalabadi, F.: On the variability of  
677 mesospheric OH emission profiles, *J. Geophys. Res.*, 112, D19109, doi:10.1029/2007JD008601,  
678 2007.

679 Pendleton, W. R., Baker, K. D., and Howlett, L. C.: Rocket-based investigations of O(<sup>3</sup>P),  
680 O<sub>2</sub>(a<sup>1</sup>Δ<sub>g</sub>) and OH\*(ν=1,2) during the solar eclipse of 26 February 1979, *J. Atm. Terr. Phys.*, 45 (7),  
681 479 – 491, doi:10.1016/S0021-9169(83)81108-8, 1983.

682 Penkett, S. A., Monks, P. S., Carpenter, L. J., Clemitschaw, K. C., Ayers, G. P., Gillett, R. W.,  
683 Galbally, I. E., and Meyer, C. P.: Relationships between ozone photolysis rates and peroxy radical  
684 concentrations in clean marine air over the Southern Ocean, *J. Geophys. Res.*, 102(D11), 12805–  
685 12817, doi:10.1029/97JD00765, 1997.

686 Penkett, S. A., Reeves, C. E., Bandy, B. J., Kent, J. M., and Richer, H. R.: Comparison of  
687 calculated and measured peroxide data collected in marine air to investigate prominent features of  
688 the annual cycle of ozone in the troposphere, *J. Geophys. Res.*, 103(D11), 13377–13388,  
689 doi:10.1029/97JD02852, 1998.

690 Platt, U., Perner, D., and Pätz, H. W.: Simultaneous measurement of atmospheric CH<sub>2</sub>O,  
691 O<sub>3</sub>, and NO<sub>2</sub> by differential optical absorption, *J. Geophys. Res.*, 84(C10), 6329–6335,  
692 doi:10.1029/JC084iC10p06329, 1979.

693 Pyle, J. A., Zavody, A. M., Harries, J. E., and Moffat, P. H.: Derivation of OH concentration  
694 from satellite infrared measurements of NO<sub>2</sub> and HNO<sub>3</sub>, *Nature*, 305, 690–692,  
695 doi:10.1038/305690a0, 1983.

696 Pyle, J. A., and Zavody, A. M.: The derivation of hydrogen containing radical concentrations  
697 from satellite data sets, *Q. J. R. Meteorol. Soc.*, 111, 993–1012, doi:10.1002/qj.49711147005,  
698 1985.

699 Pickett, H. M., and Peterson, D. B.: Comparison of measured stratospheric OH with  
700 prediction, *J. Geophys. Res.*, 101(D11), 16789–16796, doi: 10.1029/96JD01168, 1996.

701 Pickett, H. M., Drouin, B. J., Carty, T., Salawitch, R. J., Fuller, R. A., Perun, V. S., Livesey,  
702 N. J., Waters, J. W., Stachnik, R. A., Sander, S. P., Traub, W. A., Jucks, K. W., and Minschwaner,  
703 K.: Validation of Aura Microwave Limb Sounder OH and HO<sub>2</sub> measurements, *J. Geophys. Res.*,  
704 113, D16S30, doi:10.1029/2007JD008775, 2008.

705 Rasch, P. J., Boville, B. A., and Brasseur, G. P.: A three-dimensional general circulation  
706 model with coupled chemistry for the middle atmosphere, *J. Geophys. Res.*, 100(D5), 9041–9071,  
707 doi: 10.1029/95JD00019, 1995.

708 Russell, J. P., and Lowe, R. P.: Atomic oxygen profiles (80–94 km) derived from Wind  
709 Imaging Interferometer/Upper Atmospheric Research Satellite measurements of the hydroxyl  
710 airglow: 1. Validation of technique, *J. Geophys. Res.*, 108, 4662, doi:10.1029/2003JD003454, D21,  
711 2003.

712 Schwartz, M., Froidevaux, L., Livesey, N., and Read, W.: MLS/Aura Level 2 Ozone (O<sub>3</sub>)  
713 Mixing Ratio V004, Greenbelt, MD, USA, Goddard Earth Sciences Data and Information Services  
714 Center (GES DISC), accessed 13.07.16, doi:10.5067/AURA/MLS/DATA2017, 2015.

715 Scinocca, J. F., McFarlane, N. A., Lazare, M., Li, J., Plummer, D.: The CCCma third  
716 generation AGCM and its extension into the middle atmosphere, *Atmos. Chem. Phys.*, 8, 7055-  
717 7074, doi:10.5194/acp-8-7055-2008, 2008.

718 Shimazaki, T.: Minor Constituents in the Middle Atmosphere, D. Reidel, Norwell, Mass.,  
719 USA, 444 pp., 1985.

720 Siskind, D. E., Marsh, D. R., Mlynczak, M. G., Martin-Torres, F. J., and Russell III, J. M.:  
721 Decreases in atomic hydrogen over the summer pole: Evidence for dehydration from polar  
722 mesospheric clouds?, *Geophys. Res. Lett.*, 35, L13809, doi:10.1029/2008GL033742, 2008.

723 Siskind D. E., Mlynczak, M. G., Marshall, T., Friedrich, M., Gumbel, J.: Implications of odd  
724 oxygen observations by the TIMED/SABER instrument for lower D region ionospheric modeling, *J.*  
725 *Atmos. Sol. Terr. Phys.*, 124, 63–70, doi: 10.1016/j.jastp.2015.01.014, 2015.

726 Smith, A. K., Marsh, D. R., Mlynczak, M. G., and Mast, J. C.: Temporal variations of atomic  
727 oxygen in the upper mesosphere from SABER, *J. Geophys. Res.*, 115, D18309,  
728 doi:10.1029/2009JD013434, 2010.

729 Sobanski, N., Tang, M. J., Thieser, J., Schuster, G., Pöhler, D., Fischer, H., Song, W.,  
730 Sauvage, C., Williams, J., Fachinger, J., Berkes, F., Hoor, P., Platt, U., Lelieveld, J., and Crowley,  
731 J. N.: Chemical and meteorological influences on the lifetime of NO<sub>3</sub> at a semi-rural mountain site  
732 during PARADE, *Atmos. Chem. Phys.*, 16, 4867-4883, doi:10.5194/acp-16-4867-2016, 2016.

733 Solomon, S., Rusch, D. W., Gerard, J.-C., Reid, G. C., and Crutzen, P. J.: The effect of  
734 particle precipitation events on the neutral and ion chemistry of the middle atmosphere. 2. Odd  
735 hydrogen, *Planet. Space Sci.*, 29, 885–892, 1981.

736           Solomon, P., Connor, B., Barrett, J., Mooney, T., Lee, A., and Parrish, A.: Measurements of  
737           stratospheric ClO over Antarctica in 1996–2000 and implications for ClO dimer chemistry,  
738           Geophys. Res. Lett., 29(15), 1708, doi:10.1029/2002GL015232, 2002.

739           Sonnemann, G., Kremp, C., Ebel, A., and Berger, U.: A three-dimensional dynamic model of  
740           minor constituents of the mesosphere, *Atmos. Environ.*, 32, 3157–3172, doi:10.1016/S1352-  
741           2310(98)00113-7, 1998.

742           Sonnemann, G. R., Grygalashvily, M., Hartogh, P., and Jarchow, C.: Behavior of  
743           mesospheric ozone under nearly polar night conditions, *Adv. Space Res.*, 38, 2402–2407,  
744           doi:10.1016/j.asr.2006.09.011, 2006.

745           Sonnemann, G. R., Hartogh, P., Jarchow, C., Grygalashvily, M., and Berger, U.: On the  
746           winter anomaly of the night-to-day ratio of ozone in the middle to upper mesosphere in middle to  
747           high latitudes, *Adv. Space Res.*, 40, 846–854, doi:10.1016/j.asr.2007.01.039, 2007.

748           Sonnemann, G. R., Hartogh, P., Berger, U., and Grygalashvily, M.: Hydroxyl layer: trend of  
749           number density and intra-annual variability *Ann. Geophys.*, 33, 749–767, doi:10.5194/angeo-33-  
750           749-2015, 2015.

751           Swenson, G. R., and Gardner, C. S.: Analytical models for the responses of the  
752           mesospheric OH\* and Na layers to atmospheric gravity waves, *J. Geophys. Res.*, 103(D6), 6271–  
753           6294, doi:10.1029/97JD02985, 1998.

754           Solomon, P., Connor, B., Barrett, J., Mooney, T., Lee, A., and Parrish, A.: Measurements of  
755           stratospheric ClO over Antarctica in 1996–2000 and implications for ClO dimer chemistry,  
756           Geophys. Res. Lett., 29(15), 1708, doi:10.1029/2002GL015232, 2002.

757           Stedman, D. H., Chameides, W., and Jackson, J. O.: Comparison of experimental and  
758           computed values for  $J(\text{NO}_2)$ , *Geophys. Res. Lett.*, 2(1), 22-25, doi:1029/GL002i001p00022, 1975.

759           Stimpfle, R. M., Wilmouth, D. M., Salawitch, R. J., and Anderson, J. G.: First measurements  
760           of ClOOCl in the stratosphere: The coupling of ClOOCl and ClO in the Arctic polar vortex, *J.*  
761           *Geophys. Res.*, 109, D03301, doi:10.1029/2003JD003811, 2004.

762           Sumińska-Ebersoldt, O., Lehmann, R., Wegner, T., Grooß, J.-U., Hösen, E., Weigel, R.,  
763           Frey, W., Griessbach, S., Mitev, V., Emde, C., Volk, C. M., Borrmann, S., Rex, M., Stroh, F., and  
764           von Hobe, M.: ClOOCl photolysis at high solar zenith angles: analysis of the RECONCILE self-  
765           match flight, *Atmos. Chem. Phys.*, 12, 1353-1365, doi:10.5194/acp-12-1353-2012, 2012.

766 Thomas, R. J.: Atomic hydrogen and atomic oxygen density in the mesosphere region:  
767 Global and seasonal variations deduced from Solar Mesosphere Explorer near-infrared emissions,  
768 *J. Geophys. Res.*, 95, 16,457–16,476, doi:10.1029/JD095iD10p16457, 1990.

769 Tulet, P., Grini, A., Griffin, R. J., and Petitcol, S.: ORILAM-SOA: A computationally efficient  
770 model for predicting secondary organic aerosols in three-dimensional atmospheric models, *J.*  
771 *Geophys. Res.*, 111, D23208, doi:10.1029/2006JD007152, 2006.

772 von Hobe, M., Grooß, J.-U., Müller, R., Hrechanyy, S., Winkler, U., and Stroh, F.: A re-  
773 evaluation of the ClO/Cl<sub>2</sub>O<sub>2</sub> equilibrium constant based on stratospheric in-situ observations,  
774 *Atmos. Chem. Phys.*, 5, 693-702, doi:10.5194/acp-5-693-2005, 2005.

775 von Hobe, M., Salawitch, R. J., Canty, T., Keller-Rudek, H., Moortgat, G. K., Grooß, J.-U.,  
776 Müller, R., and Stroh, F.: Understanding the kinetics of the ClO dimer cycle, *Atmos. Chem. Phys.*,  
777 7, 3055-3069, doi:10.5194/acp-7-3055-2007, 2007.

778 Walcek, C. J., and N. M. Aleksic [\(1998\)](#), A simple but accurate mass conservative, peak  
779 preserving, mixing ratio bounded advection algorithm with Fortran code, *Atmos. Environm.*, 32,  
780 3863-3880, [1998](#).

781 Walcek, C. J. [\(2000\)](#), Minor flux adjustment near mixing ratio extremes for simplified yet  
782 highly accurate monotonic calculation of tracer advection, *J. Geophys. Res.*, 105, 9335-9348, [2000](#).

784 Wang, S., Pickett, H., Livesey, N., and Read, W.: MLS/Aura Level 2 Hydroperoxy (HO<sub>2</sub>)  
785 Mixing Ratio V004, Greenbelt, MD, USA, Goddard Earth Sciences Data and Information Services  
786 Center (GES DISC), accessed 13.07.16, doi:10.5067/AURA/MLS/DATA2013, 2015a.

787 Wang, S., Livesey, N., and Read, W.: MLS/Aura Level 2 Hydroxyl (OH) Mixing Ratio V004,  
788 Greenbelt, MD, USA, Goddard Earth Sciences Data and Information Services Center (GES DISC),  
789 accessed 13.07.16, doi:10.5067/AURA/MLS/DATA2018, 2015b.

790 Webster, C. R., May, R. D., Toumi, R., and Pyle, J. A.: Active nitrogen partitioning and the  
791 nighttime formation of N<sub>2</sub>O<sub>5</sub> in the stratosphere: Simultaneous in situ measurements of NO, NO<sub>2</sub>,  
792 HNO<sub>3</sub>, O<sub>3</sub>, and N<sub>2</sub>O using the BLISS diode laser spectrometer, *J. Geophys. Res.*, 95(D9), 13851–  
793 13866 doi: 10.1029/JD095iD09p13851, 1990.

794 Wetzel, G., Oelhaf, H., Kirner, O., Friedl-Vallon, F., Ruhnke, R., Ebersoldt, A., Kleinert, A.,  
795 Maucher, G., Nordmeyer, H., and Orphal, J.: Diurnal variations of reactive chlorine and nitrogen

796 oxides observed by MIPAS-B inside the January 2010 Arctic vortex, *Atmos. Chem. Phys.*, 12,  
797 6581-6592, doi:10.5194/acp-12-6581-2012, 2012.

798 Xu, J., Smith, A. K., Jiang, G., Gao, H., Wei, Y., Mlynczak, M. G. ,and Russell III, J. M.:  
799 Strong longitudinal variations in the OH nightglow, *Geophys. Res. Lett.*, 37, L21801,  
800 doi:10.1029/2010GL043972, 2010.

801 Xu, J., Gao, H., Smith, A. K., and Zhu, Y.: Using TIMED/SABER nightglow observations to  
802 investigate hydroxyl emission mechanisms in the mesopause region, *J. Geophys. Res.*, 117,  
803 D02301, doi:10.1029/2011JD016342, 2012.

804

805

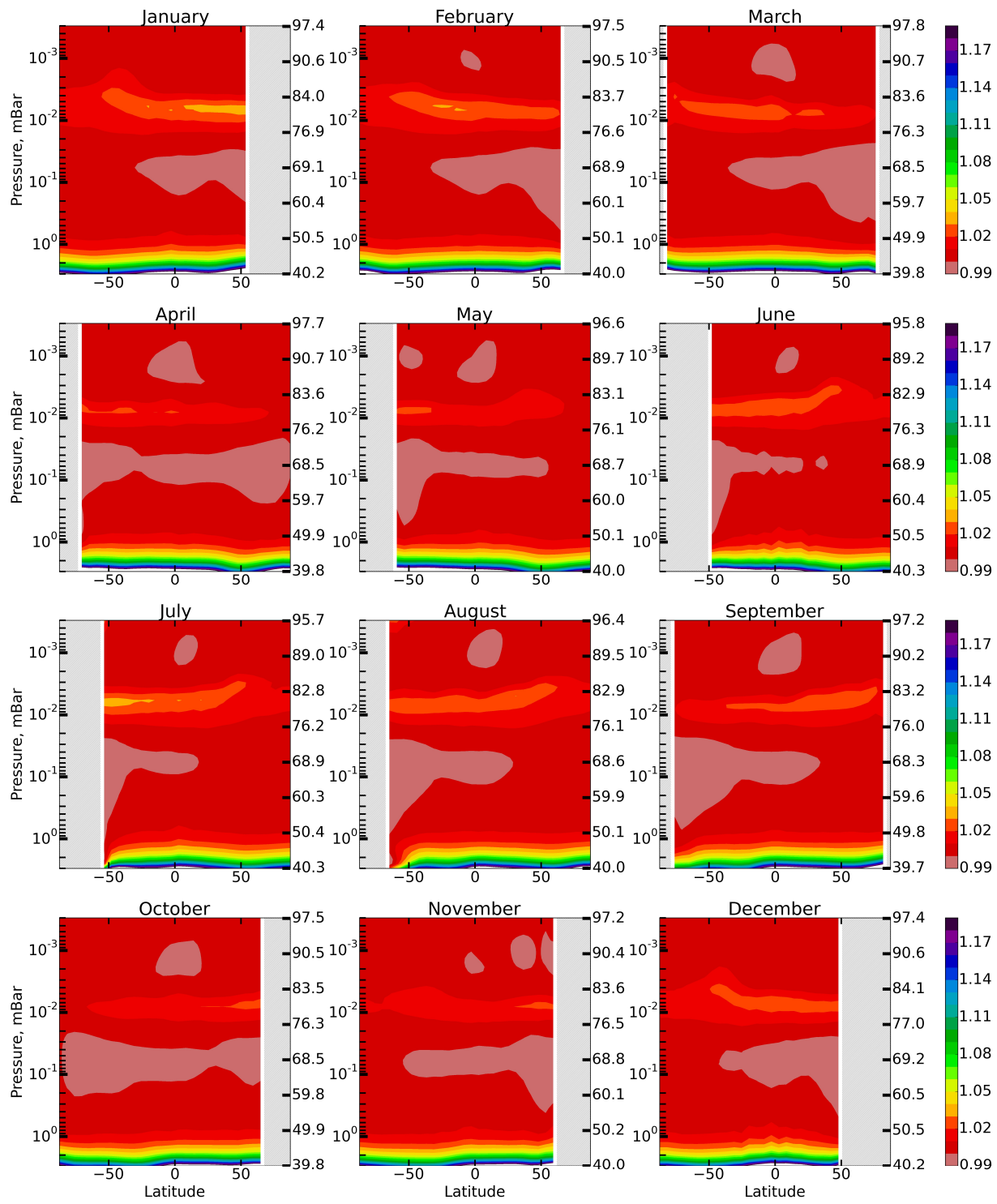
806 **Table 1.** List of reactions with corresponding reaction rates from Burkholder et al. (2015).  
807

1	$O(^1D) + O_2 \rightarrow O + O_2$	22	$OH + O_3 \rightarrow O_2 + HO_2$	43	$NO_2 + O_3 \rightarrow NO_3 + O_2$
2	$O(^1D) + N_2 \rightarrow O + N_2$	23	$HO_2 + O_3 \rightarrow OH + 2O_2$	44	$N + OH \rightarrow NO + H$
3	$O(^1D) + O_3 \rightarrow O_2 + 2O$	24	$H + OH + N_2 \rightarrow H_2O + N_2$	45	$NO + HO_2 \rightarrow NO_2 + OH$
4	$O(^1D) + O_3 \rightarrow 2O_2$	25	$OH + H_2 \rightarrow H_2O + H$	46	$H + NO_2 \rightarrow OH + NO$
5	$O(^1D) + N_2O \rightarrow 2NO$	26	$OH + OH \rightarrow H_2O + O$	47	$NO_3 + NO \rightarrow 2NO_2$
6	$O(^1D) + N_2O \rightarrow N_2 + O_2$	27	$OH + OH + M \rightarrow H_2O_2 + M$	48	$N + NO \rightarrow N_2 + O$
7	$O(^1D) + H_2O \rightarrow 2OH$	28	$OH + HO_2 \rightarrow H_2O + O_2$	49	$N + NO_2 \rightarrow N_2O + O$
8	$O(^1D) + H_2 \rightarrow H + OH$	29	$H_2O_2 + OH \rightarrow H_2O + HO_2$	50	$O_2 + h\nu \rightarrow 2O$
9	$O(^1D) + CH_4 \rightarrow CH_3 + OH$	30	$HO_2 + HO_2 \rightarrow H_2O_2 + O_2$	51	$O_2 + h\nu \rightarrow O + O(^1D)$
10	$O(^1D) + CH_4 \rightarrow H_2 + CH_2O$	31	$HO_2 + HO_2 + M \rightarrow H_2O_2 + O_2 + M$	52	$O_3 + h\nu \rightarrow O_2 + O$
11	$O + O + M \rightarrow O_2 + M$	32	$CH_3 + O \rightarrow CH_2O + H$	53	$O_3 + h\nu \rightarrow O_2 + O(^1D)$
12	$O + O_2 + M \rightarrow O_3 + M$	33	$OH + CO \rightarrow H + CO_2$	54	$N_2 + h\nu \rightarrow 2N$
13	$O + O_3 \rightarrow O_2 + O_2$	34	$CH_4 + OH \rightarrow CH_3 + H_2O$	55	$NO + h\nu \rightarrow N + O$
14	$H + HO_2 \rightarrow 2OH$	35	$CH_3 + O_2 + M \rightarrow CH_3O_2 + M$	56	$NO_2 + h\nu \rightarrow NO + O$
15	$H + HO_2 \rightarrow H_2O + O$	36	$O_3 + N \rightarrow NO + O_2$	57	$N_2O + h\nu \rightarrow N_2 + O(^1D)$
15	$H + HO_2 \rightarrow H_2 + O_2$	37	$NO_3 + O \rightarrow NO_2 + O_2$	58	$N_2O + h\nu \rightarrow N + NO$
17	$OH + O \rightarrow H + O_2$	38	$O + NO + M \rightarrow NO_2 + M$	59	$H_2O + h\nu \rightarrow H + OH$
18	$HO_2 + O \rightarrow OH + O_2$	39	$NO_2 + O \rightarrow NO + O_2$	60	$CH_4 + h\nu \rightarrow CH_2 + H_2$
19	$H_2O_2 + O \rightarrow OH + HO_2$	40	$NO_2 + O + M \rightarrow NO_3 + M$	61	$H_2O_2 + h\nu \rightarrow 2OH$
20	$H + O_2 + M \rightarrow HO_2 + M$	41	$N + O_2 \rightarrow NO + O$	62	$NO_3 + h\nu \rightarrow NO_2 + O$
21	$H + O_3 \rightarrow OH + O_2$	42	$NO + O_3 \rightarrow NO_2 + O_2$	63	$CO_2 + h\nu \rightarrow CO + O$

808

809

810

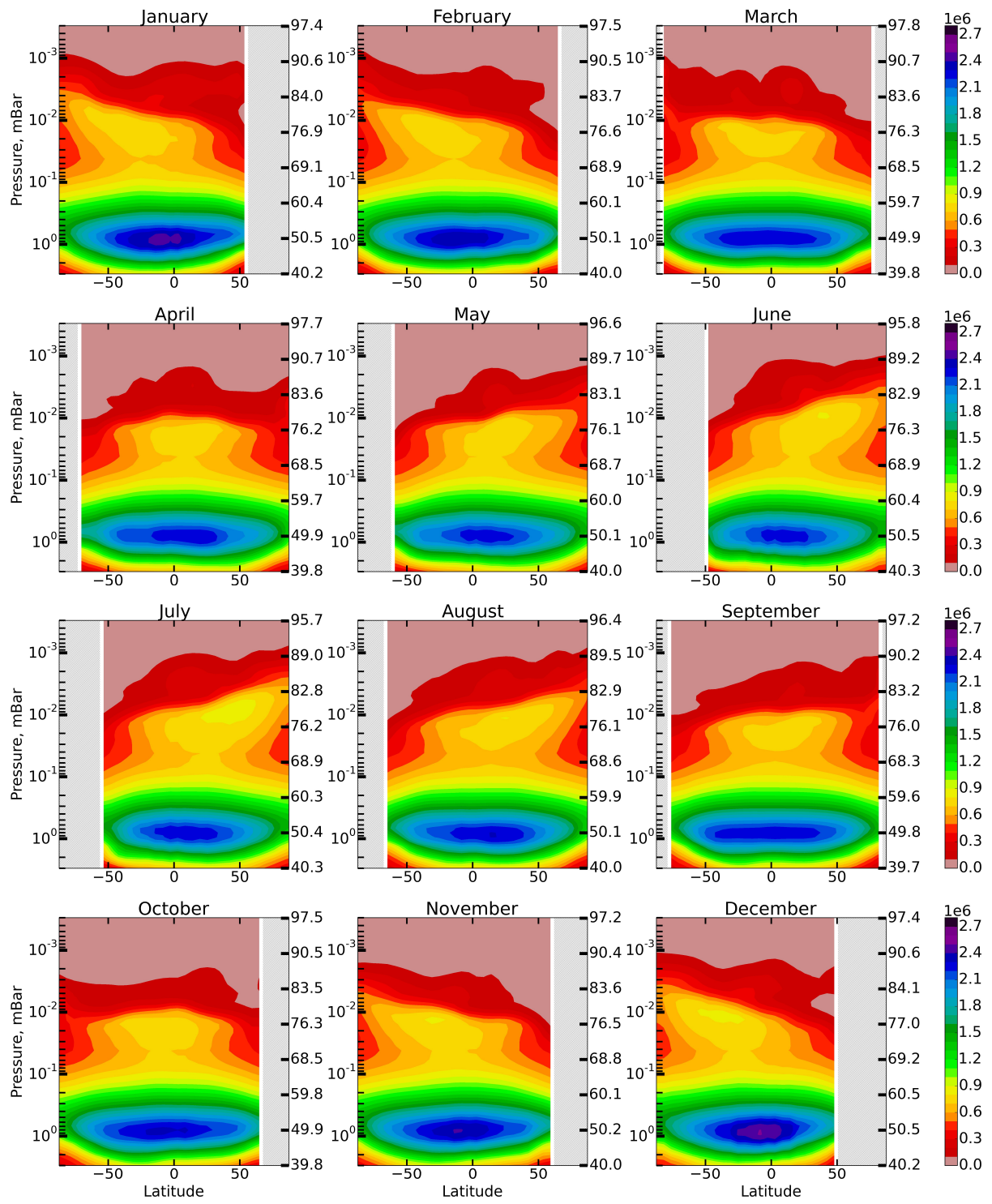


811

812 Figure 1. Daytime monthly averaged zonal mean  $F$  distributions.

813

814

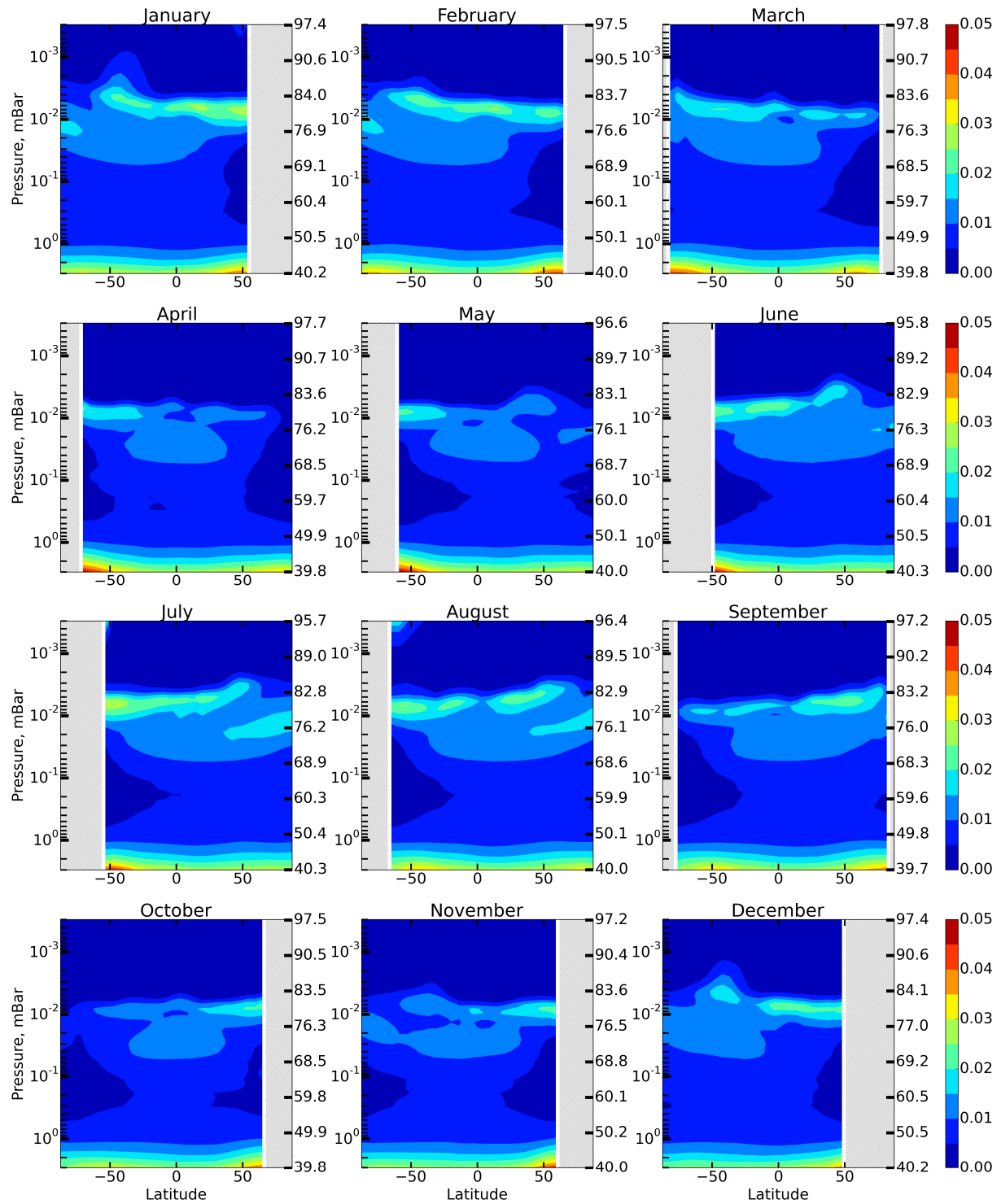


815

816 Figure 2. Daytime monthly averaged zonal mean  $P_{OH}$  distributions (in  $\text{cm}^{-3}\text{s}^{-1}$ ).

817

818



819

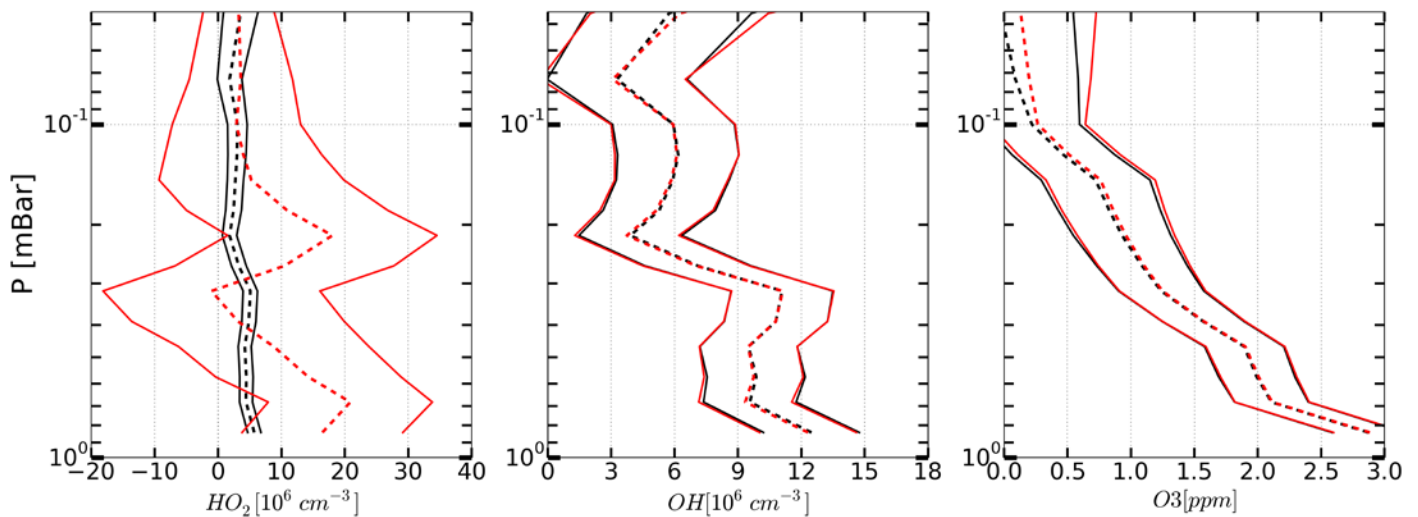
820

821 Figure 3. Daytime monthly averaged zonal mean  $P_{OH}^{H_2O} / P_{OH}$  distributions.

822

823

16:03 15.01.2005 UT 37° 3' N 3° 7' E



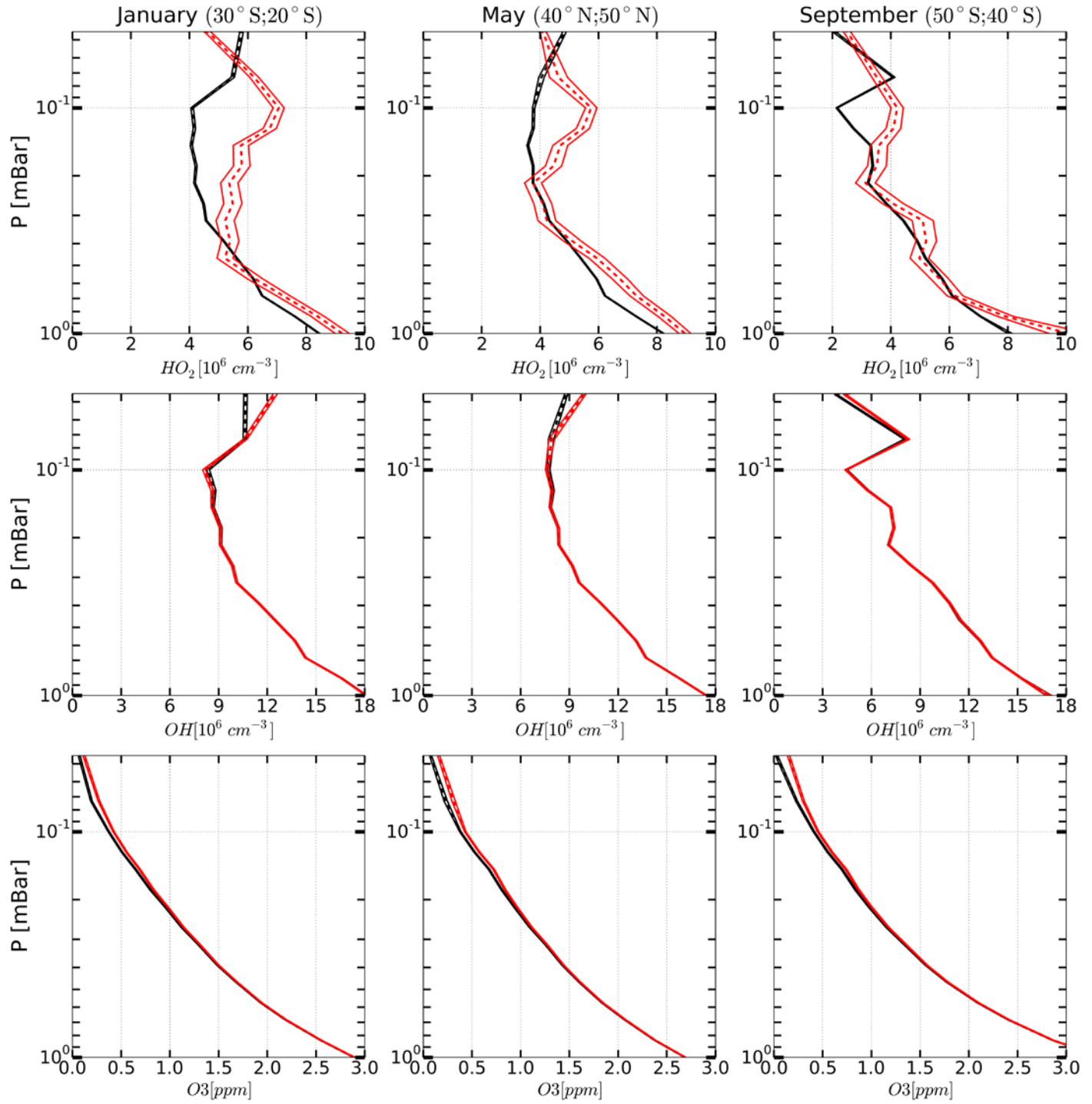
824

825

826 Figure 4. Example of OH,  $HO_2$  and  $O_3$  vertical profiles measured (red curves) on 15 January 2005  
 827 at 16.03 UT,  $37^{\circ}3'N$ ,  $3^{\circ}7'E$  and corresponding retrieved profiles (black curves). Solid curves:  
 828 boundaries of the 65% confident intervals, dashed curves: medians.

829

830

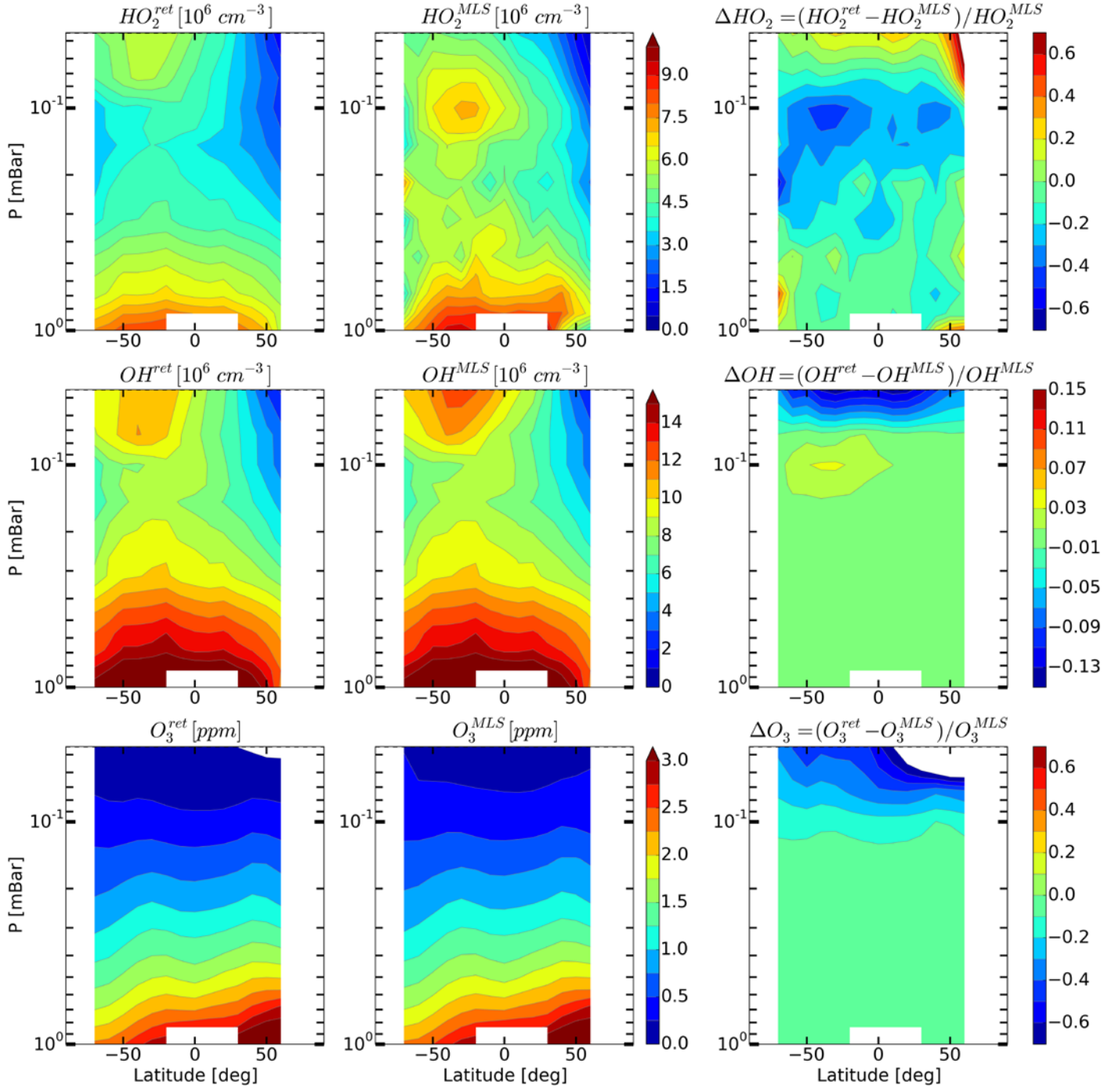


831

832

833 Figure 5. Examples of monthly averaged zonal mean vertical profiles of OH, HO<sub>2</sub> and O<sub>3</sub> measured  
 834 (red curves) in January, May and March 2005 and corresponding retrieved profiles (black curves).  
 835 Solid curves: boundaries of the 65% confident intervals, dashed curves: medians.

836

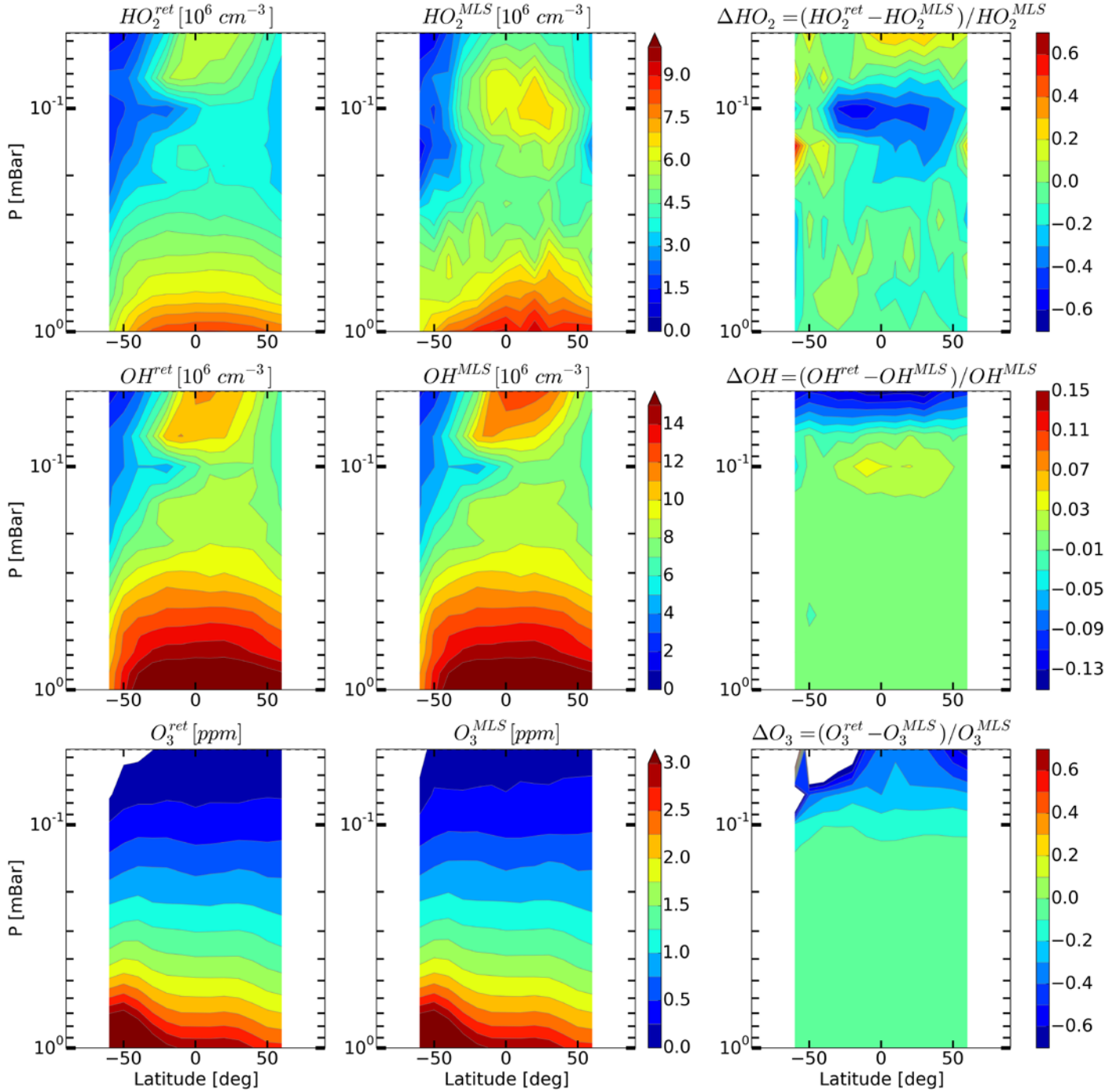


837

838

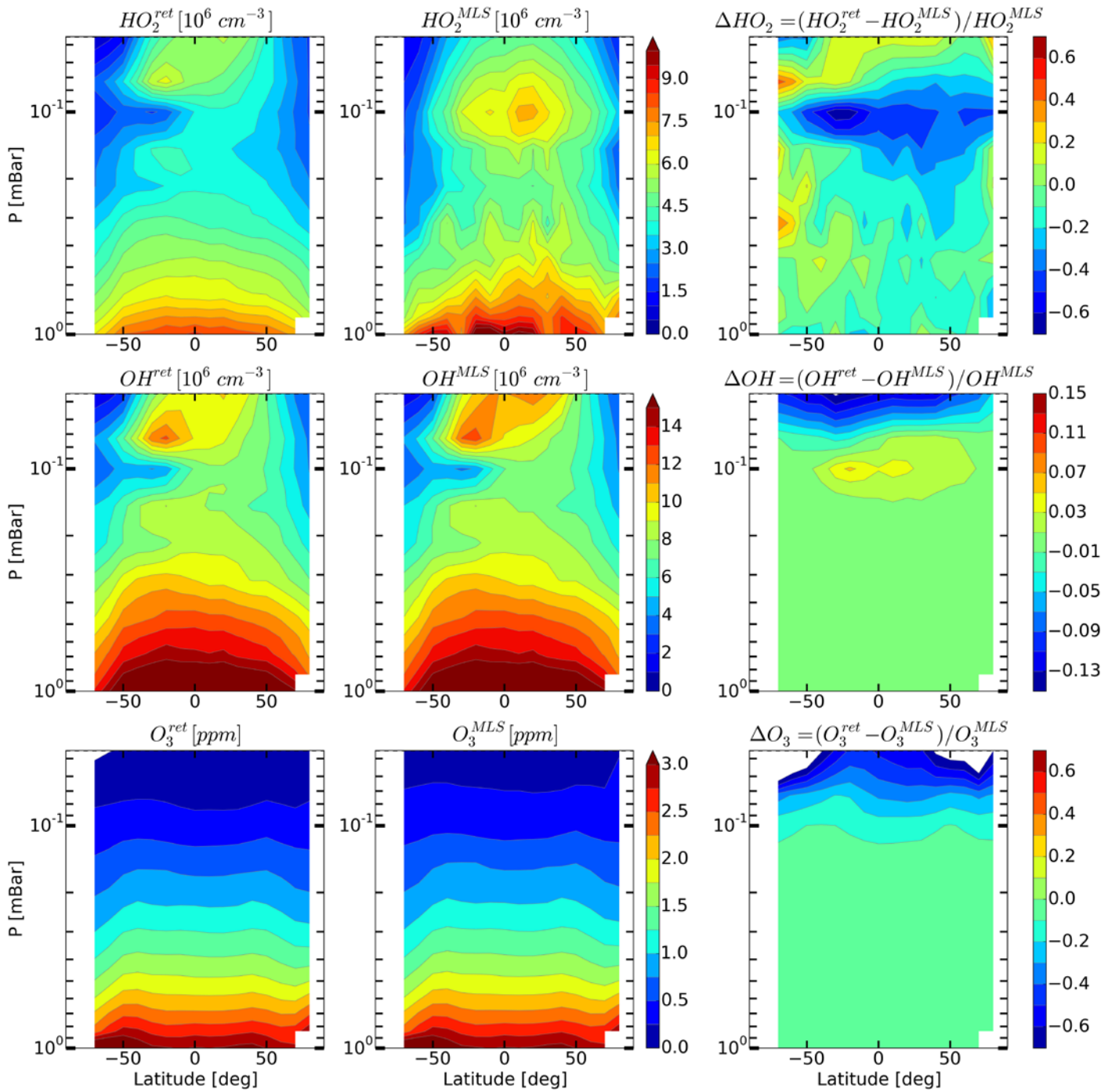
839 Figure 6. Daytime monthly averaged zonal mean retrieved (left column) and measured (middle  
 840 column) distributions of HO<sub>2</sub>, OH, and O<sub>3</sub> and their relative difference (right column) in January  
 841 2005.

842



846 Figure 7. Daytime monthly averaged zonal mean retrieved (left column) and measured (middle  
 847 column) distributions of HO<sub>2</sub>, OH, and O<sub>3</sub> and their relative difference (right column) for May 2005.

850

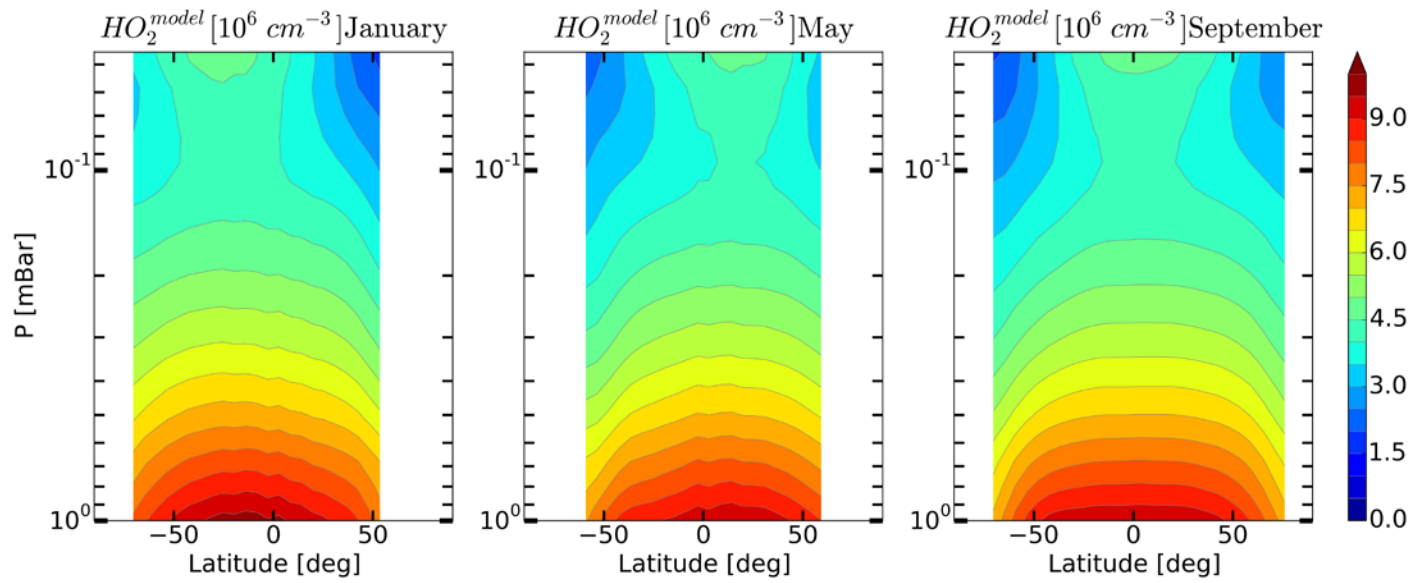


851

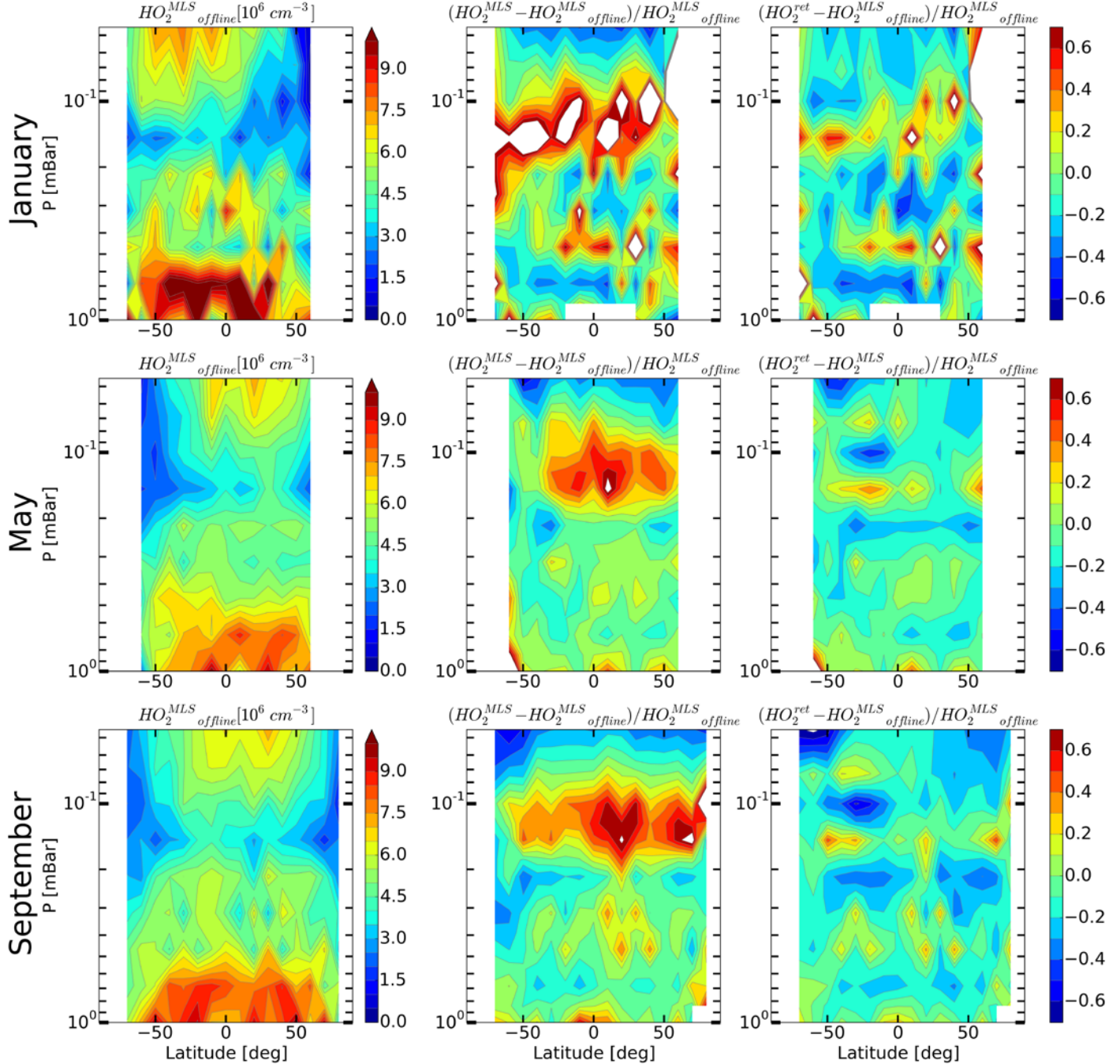
852

853 Figure 8. Daytime monthly averaged zonal mean retrieved (left column) and measured (middle  
 854 column) distributions of HO<sub>2</sub>, OH, and O<sub>3</sub> and their relative difference (right column) for September  
 855 2005.

856



857  
858 Figure 9. Daytime monthly averaged zonal mean model distributions of HO<sub>2</sub> for January, May, and  
859 September.  
860  
861



865 Figure 10. Daytime mean monthly averaged distributions of  $HO_2$  retrieved by Millán et al. (2015)  
 866 and relative differences  $(\langle HO_2^{MLS} \rangle - \langle HO_2^{offline} \rangle) / \langle HO_2^{MLS} \rangle$  and  
 867  $(\langle HO_2^{ret} \rangle - \langle HO_2^{offline} \rangle) / \langle HO_2^{MLS} \rangle$ .